Title	Integrated in vitro and in silico modelling delineates the molecular effects of a synbiotic regimen on colorectal cancer-derived cells
Author(s)	Greenhalgh, Kacy; Ramiro-Garcia, Javier; Heinken, Almut; Ullmann, Pit; Bintener, Tamara; Pires Pacheco, Maria; Baginska, Joanna; Shah, Pranjul; Frachet, Audrey; Halder, Rashi; Fritz, Joëlle V.; Sauter, Thomas; Thiele, Ines; Haan, Serge; Letellier, Elisabeth; Wilmes, Paul
Publication Date	2019-04-30
Publication Information	Greenhalgh, Kacy, Ramiro-Garcia, Javier, Heinken, Almut, Ullmann, Pit, Bintener, Tamara, Pires Pacheco, Maria, Baginska, Joanna, Shah, Pranjul, Frachet, Audrey, Halder, Rashi, Fritz, Joëlle V. Sauter, Thomas, Thiele, Ines, Haan, Serge, Letellier, Elisabeth, Wilmes, Paul. (2019). Integrated In Vitro and In Silico Modeling Delineates the Molecular Effects of a Synbiotic Regimen on Colorectal-Cancer-Derived Cells. Cell Reports, 27(5), 1621-1632. doi:10.1016/j.celrep.2019.04.001
Publisher	Cell Press
Link to publisher's version	https://doi.org/10.1016/j.celrep.2019.04.001
Item record	http://hdl.handle.net/10379/16385
DOI	http://dx.doi.org/10.1016/j.celrep.2019.04.001

Cell Reports

Resource

Integrated *In Vitro* and *In Silico* Modeling Delineates the Molecular Effects of a Synbiotic Regimen on Colorectal-Cancer-Derived Cells

Graphical Abstract

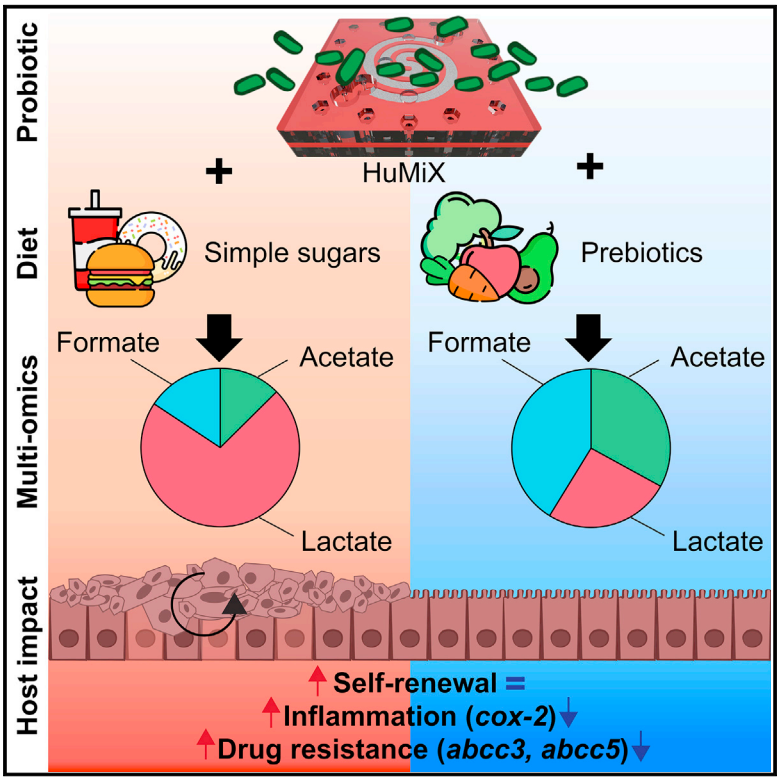

Highlights

- Modeling of combinatorial effects of pre- and probiotic (synbiotic) regimens on cancer
- HuMiX represents diet-microbiome-human interactions
- The synbiotic regimen reduces molecular hallmarks of cancer
- Cocktail of synbiotic-derived small molecules limits cancer self-renewal capacity

Authors

Kacy Greenhalgh, Javier Ramiro-Garcia, Almut Heinken, ..., Serge Haan, Elisabeth Letellier, Paul Wilmes

Correspondence

paul.wilmes@uni.lu

In Brief

The use of specific diets that promote the growth of beneficial microorganisms together with such microorganisms may help treat such diseases as colorectal cancer. Greenhalgh et al. show that one such synbiotic regimen induces downregulation of pro-carcinogenic and drug resistance genes as well as metabolic changes that affect the growth of cancer cells.

Greenhalgh et al., 2019, Cell Reports *27*, 1621–1632
April 30, 2019
https://doi.org/10.1016/j.celrep.2019.04.001

CellPress

Cell Reports
Resource

Integrated *In Vitro* and *In Silico* Modeling Delineates the Molecular Effects of a Synbiotic Regimen on Colorectal-Cancer-Derived Cells

Kacy Greenhalgh,[1] Javier Ramiro-Garcia,[1] Almut Heinken,[1,3] Pit Ullmann,[2] Tamara Bintener,[2] Maria Pires Pacheco,[2] Joanna Baginska,[1,4] Pranjul Shah,[1] Audrey Frachet,[1] Rashi Halder,[1] Joëlle V. Fritz,[1,5] Thomas Sauter,[2] Ines Thiele,[1,2] Serge Haan,[2] Elisabeth Letellier,[2] and Paul Wilmes[1,6,*]

[1]Luxembourg Centre for Systems Biomedicine, University of Luxembourg, Belvaux 4367, Luxembourg
[2]Life Sciences Research Unit, University of Luxembourg, Belvaux 4367, Luxembourg
[3]Present address: School of Medicine, National University of Ireland, Galway, University Road, Galway, Ireland
[4]Present address: Broad Institute of MIT and Harvard, Cambridge, MA, USA
[5]Present address: Centre Hospitalier Luxembourg, Luxembourg 1210, Luxembourg
[6]Lead Contact
*Correspondence: paul.wilmes@uni.lu
https://doi.org/10.1016/j.celrep.2019.04.001

SUMMARY

By modulating the human gut microbiome, prebiotics and probiotics (combinations of which are called synbiotics) may be used to treat diseases such as colorectal cancer (CRC). Methodological limitations have prevented determining the potential combinatorial mechanisms of action of such regimens. We expanded our HuMiX gut-on-a-chip model to co-culture CRC-derived epithelial cells with a model probiotic under a simulated prebiotic regimen, and we integrated the multi-omic results with *in silico* metabolic modeling. In contrast to individual prebiotic or probiotic treatments, the synbiotic regimen caused downregulation of genes involved in procarcinogenic pathways and drug resistance, and reduced levels of the oncometabolite lactate. Distinct ratios of organic and short-chain fatty acids were produced during the simulated regimens. Treatment of primary CRC-derived cells with a molecular cocktail reflecting the synbiotic regimen attenuated self-renewal capacity. Our integrated approach demonstrates the potential of modeling for rationally formulating synbiotics-based treatments in the future.

INTRODUCTION

The human gut microbiome is increasingly recognized as playing a major role in human health and disease (Pflughoeft and Versalovic, 2012). Modulation of the gut microbiome using prebiotics (non-digestible nutrients, e.g., dietary fiber, that promote the growth of beneficial microorganisms in the host [Hutkins et al., 2016]), probiotics (live microorganisms that, when administered in adequate amounts, confer health benefits to the host [FAO and WHO, 2002]), or combinations thereof (synbiotics) is regarded as a means to prevent microbiome-linked diseases, such as colorectal cancer (CRC) (Rafter et al., 2007; Raman et al., 2013). In addition, such dietary regimens may act as supportive therapeutic options in the management of diseases (DiMarco-Crook and Xiao, 2015; Ho et al., 2018). However, although microbiome-modulating therapeutics hold great promise (Valencia et al., 2017), dietary regimens are not formally integrated in current treatment plans (Caccialanza et al., 2016).

The health benefits attributed to dietary fiber and prebiotics in the prevention of CRC (Murphy et al., 2012; Raman et al., 2013) are mainly attributed to the metabolic activity of the gut microbiome resulting in specific fermentation products, such as lactate and short-chain fatty acids (SCFAs) and not to the fiber itself (Koh et al., 2016; Sharma and Shukla, 2016). Thereby, common dietary guidance for CRC patients is to consume a diet rich in fiber (Song et al., 2018). However, due to the limitations of existing methodologies, in particular the lack of means to study the molecular effects of diet-microbiome-host interactions (Read and Holmes, 2017), limited evidence exists on the therapeutic benefits of pre- and probiotics in CRC treatment. A limited number of studies have focused on inflammatory and proliferative signatures in CRC cells, but these have not assessed the linked changes in gene expression or metabolism (Ho et al., 2018; Le Leu et al., 2005). Nevertheless, the results from these initial studies indicate the need for investigating the combinatorial effects of synbiotics at the molecular level as they may be harnessed for therapeutic approaches in conjunction with other CRC treatments. In this context, elucidating the mechanisms of action of synbiotic regimens in relation to their possible influence on chemotherapy resistance (Ho et al., 2018; Niero et al., 2014) may prove particularly valuable to improve the efficacy of current anti-cancer treatments.

Due to the fact that CRC is mostly driven by environmental factors (e.g., diet) (Blot and Tarone, 2015; Rothenberg, 2015) and a broad range of mutations (Armaghany et al., 2012), it is challenging to recapitulate the complexity of the disease using only one specific model (Young et al., 2013). Differences in diet, gut topology, genetic background, and microbiome composition, as well as the immune system, render widely used murine models questionable for investigating mechanisms underlying human host-microbiome interactions (Fritz et al., 2013; Hildebrand

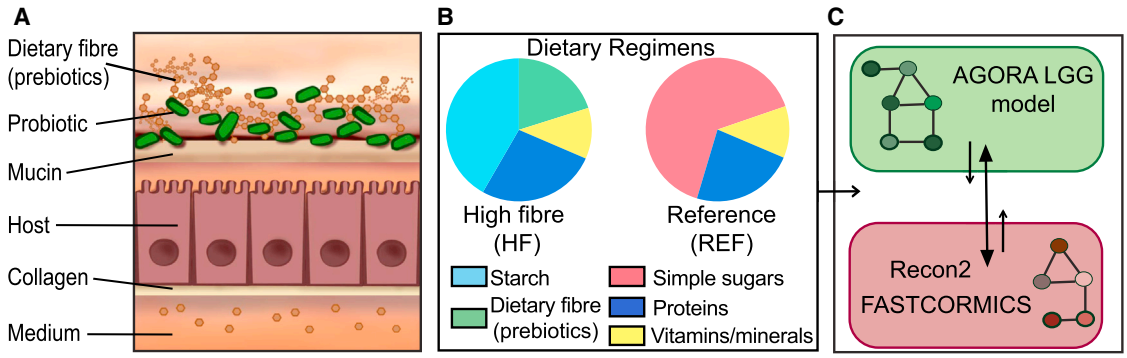

Figure 1. Integrated *In Vitro* and *In Silico* Modeling of the Interactions between Dietary Fiber, a Probiotic, and Human Cells

(A) Conceptual diagram of the *in vitro* human cells-microbe gut model HuMiX. The probiotic is cultured in the presence of the simulated dietary regimens in the top chamber separated via a nanoporous membrane from the middle chamber that houses human epithelial cells (e.g., Caco-2 cells). The bottom chamber, also separated from the middle chamber via a microporous membrane, is perfused with cell culture medium and mediates the transport of nutrients to the human cells' basal surface. Using a transwell system setup, no growth of human cells in the presence of dietary fiber compounds could be observed. See also Figure S1. In contrast, Caco-2 cells were viable when using the HuMiX model (Figure S2).

(B) Compositions of two distinct dietary regimens. The high-fiber (HF) regimen consisted of a medium high in starch and dietary fiber (including prebiotics). The reference (REF) regimen contained neither dietary fiber (or prebiotics) nor starch. Both dietary regimens contained approximately the same amount of protein and vitamins/minerals.

(C) Diagram of the *in silico* model used for the simulation of the effects of prebiotic and probiotic combinations on the human cells. The model of LGG from the AGORA modeling framework was integrated with the context-specific colon adenocarcinoma (COAD) model using Recon2 via the FASTCORMICS workflow.

et al., 2013). Although a major limitation of *in vitro* models is their reduced complexity, such models allow recapitulation of human host-microbiome interactions and thereby allow the probing of molecular exchanges between microbial and human cells and their repercussions in a representative manner (Bein et al., 2018; Paul et al., 2018). However, to study the complex and dynamic processes driving diet-host-microbiome interactions and their effects on CRC progression, *in vitro* models that allow the investigation of molecular interactions between the specific contingents are required. Moreover, when these models are complemented using *in silico* modeling, we can study specific individual metabolic reactions (e.g., via reaction fluxes), thereby linking functional potential (*in silico*) to experimental measurements (*in vitro*) (Magnúsdóttir and Thiele, 2018).

Here, we used our representative microfluidics-based human-microbial co-culture system called HuMiX (Shah et al., 2016) to obtain essential mechanistic insights into the interplay between a simulated high-fiber (HF) diet, the model probiotic *Lactobacillus rhamnosus* Gorbach-Goldin (LGG), and human CRC cells. We combined *in vitro* multi-omic data (transcriptomics and metabolomics) with *in silico* simulations by using an integrated constraint-based model (CBM) (Orth et al., 2010) of colon adenocarcinoma (COAD) cells coupled to a curated genome-scale metabolic reconstruction of LGG (Magnúsdóttir et al., 2017). In contrast to individual prebiotic or probiotic treatments, the synbiotic regimen caused downregulation of genes involved in procarcinogenic pathways and drug resistance, resulting in reduced levels of the oncometabolite lactate. *In vitro*, different ratios of organic and short-chain fatty acids were produced by the probiotic during the simulated regimens. We validated our results by testing distinct cocktails of these metabolites reflecting the different combinations on spheroid cultures generated from primary colon tumors. The treatment with a cocktail reflecting the synbiotic regimen attenuated self-renewal capacity in primary CRC-derived cells, a cellular hallmark of tumor progression and disease dissemination. Taken together, our results provide mechanistic support regarding the potential of integrating synbiotic combinations in the context of therapeutic regimens for CRC (DiMarco-Crook and Xiao, 2015; Le Leu et al., 2005). We anticipate that, in the near future, such integrative *in vitro* and *in silico* modeling could be used to develop personalized dietary treatments, including dietary guidelines and probiotic supplementation for CRC patients.

RESULTS

Establishment of an *In Vitro* and *In Silico* Model System to Study the Interactions between Dietary Fiber, Probiotics, and the Human Host

In accordance with previous reports (Niero et al., 2014), we found that a simulated dietary fiber regimen (e.g., prebiotic regimen) is incompatible with standard cell culture approaches (Figure S1). In contrast, the use of the HuMiX model allows the exposure of human cells to dietary compounds and live bacterial cells via the apical interface, thereby mimicking *in vivo* physiology and enabling the study of diet-host-microbe molecular interactions (Figure 1A). To simulate a fiber-rich prebiotic regimen, we formulated a HF medium containing major non-digestible carbohydrates and supplemented it with additional prebiotics including arabinogalactan, xylan, and soy (Gibson et al., 1988) (Figure 1B). A human cell culture medium providing the basic requirements for culture of both Caco-2 cells and LGG (Shah et al., 2016) was used as reference (REF) medium, i.e., a medium containing no dietary fiber. Using the different simulated dietary regimes (HF alone or REF alone), we studied the molecular impact of diet on bacterial and human cell physiology (measured by transcriptomics) as well as on the resulting intercellular cross-talk (metabolomics).

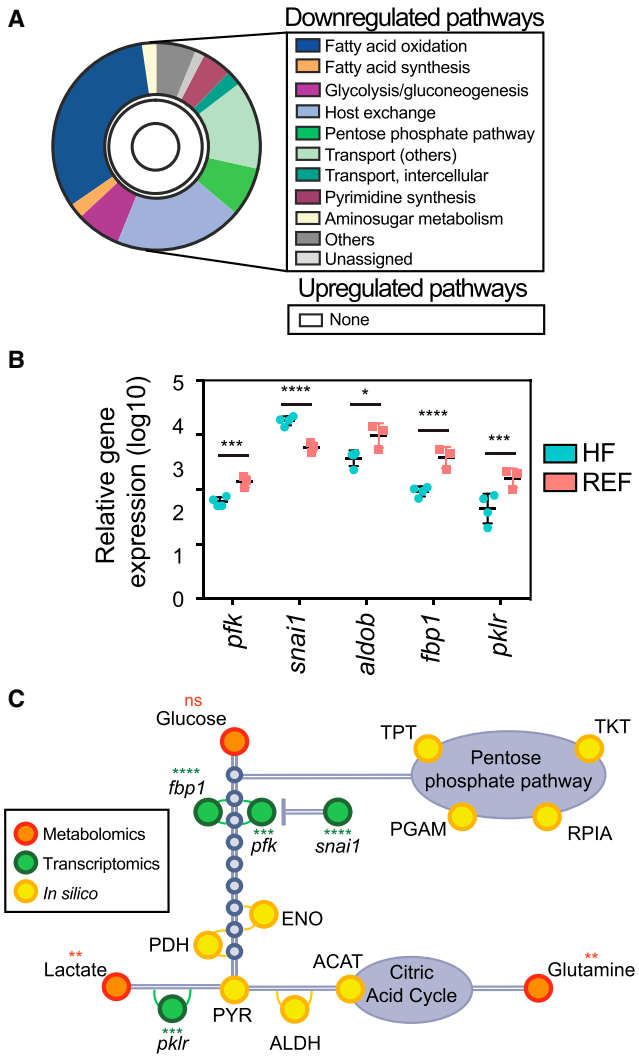

Figure 2. A Simulated HF Regimen Alone Alters the Energy Metabolism in Caco-2 Cells

(A) List of down- and upregulated differential flux span reactions in HF-exposed Caco-2 cells. The inner ring represents upregulated reactions; the outer ring represents downregulated pathways (Table S3). Each section of the plot indicates the fraction in % of all the listed pathways. See also Figure S2C.

(B and C) Caco-2 cells were grown in the HuMiX model in the presence of the simulated HF regimen or REF medium. Differentially expressed genes were calculated using the Wald test implemented in DESeq2 with Benjamini-Hochberg multiple testing correction at 0.05 significance.

(B) *In vitro* glycolysis-related genes differentially expressed in HF-exposed cells compared to REF-exposed cells. Data are shown as mean ± SD for three REF-exposed and four HF-exposed independent HuMiX experiments. *pfk*, phosphofructokinase; *aldob*, aldolase B; *fbp1*, fructo-1,6-biphosphatase; *pklr*, pyruvate kinase isozymes R and L; *snai1*, snail family transcriptional repressor 1.

(C) Integrated schematic overview of *in vitro* and *in silico* results reflecting the effects of the simulated HF regimen on Caco-2 cell metabolism and colors indicate omics type. Differences in metabolite values were obtained using Welch's t test by comparing the data from technical duplicates for two REF-exposed and three HF-exposed independent HuMiX experiments. See also Figure S2A and Table S1. *In silico* values represents differential flux span of HF-exposed and REF-exposed Caco-2 cells, summarized by assigned reaction subsystems retrieved from the Virtual Metabolic Human (VMH) database. Shown in color key: *p < 0.05; **p < 0.01; ***p < 0.0001; ****p < 0.00001; ns, not significant. PYR, pyruvate; ALDH, aldehyde dehydrogenase; ACAT, acetyl CoA; TPT, triose phosphate; TKT, transketolase; RPIA, ribose 5-phosphate isomerase; PGAM, phosphoglycerate mutase; PPM, phosphopentomutase.

To complement the *in vitro* modeling, we coupled a CBM (Orth et al., 2010) of COAD cells with a model of LGG (Magnúsdóttir et al., 2017) A context-specific model of COAD was reconstructed, starting with the genome-scale human metabolic reconstruction Recon2 (Thiele et al., 2013) and data from The Cancer Genome Atlas (TCGA) dataset (Rahman et al., 2015), as well as an extension to the FASTCORMICS workflow (Pacheco et al., 2015) that uses RNA-seq data (M.P.P., T.B., D. Ternes, D. Kulms, S.G., E.L., T.S., unpublished data) (Figure 1C). The models were further contextualized with *in vitro* data by using growth rates and secretion product ratios generated in this study. For each dietary regimen (HF alone, REF alone, HF + LGG, REF + LGG), we determined the differential flux span of each cell-type (Caco-2 and LGG), which were grouped and summarized by assigned reaction subsystems retrieved from the Virtual Metabolic Human (VMH) database (Noronha et al., 2019).

A Simulated HF Regimen Alone Affects Energy Metabolism in Caco-2 Cells

Recent studies have linked altered metabolism, through the production of oncometabolites, to tumorigenesis in CRC (Corrado et al., 2016; Morin et al., 2014). Analysis of the *in silico* differential flux spans in HF-exposed Caco-2 cells in comparison to REF-exposed cells revealed that the flux spans of 11 subsystem reactions were smaller in the COAD model when exposed to the simulated HF regimen versus the REF medium, including transport, pentose phosphate metabolism, glycolysis, and gluconeogenesis, as well as fatty acid oxidation and synthesis (Figure 2A). No COAD model reaction in Caco-2 had larger flux spans when comparing predictions from the simulated HF regimen with the REF medium (Figure 2A). Next, we analyzed whether alterations in energy metabolism affected gene regulation. Indeed, expression of several glycolytic enzymes was found to be significantly reduced in Caco-2 cells after co-culture with the simulated HF regimen (Figure 2B), including phosphofructokinase (*pfk*), aldolase B (*aldob*), fructo-1,6-biphosphatase (*fbp1*) and pyruvate kinase isozymes R and L (*pklr*) (Figure 2B). The snail family transcriptional repressor 1 (*snai1*), which regulates glycolysis by inhibiting *pfk* expression (Kim et al., 2017), was significantly increased (Figure 2B). Increased glucose, lactate, and glutamine levels promote metabolic reprogramming (Altman et al., 2016; Jang et al., 2013), and, thus, we next investigated intracellular concentrations in Caco-2 cells. *In vitro*, the intracellular lactate concentrations in Caco-2 cells were significantly reduced ($p = 2.63 \times 10^{-3}$) in the presence of the simulated HF regimen compared with the REF condition (Figure S2A and Table S1). Furthermore, a downregulation (although not significant) of lactate transporters was observed in Caco-2 cells exposed to the simulated HF regimen compared with the REF medium (Figure S2B). Additionally, the concentration of intracellular glucose was decreased (although not significant), while the concentration of glutamine was significantly increased ($p = 2.43 \times 10^{-3}$)

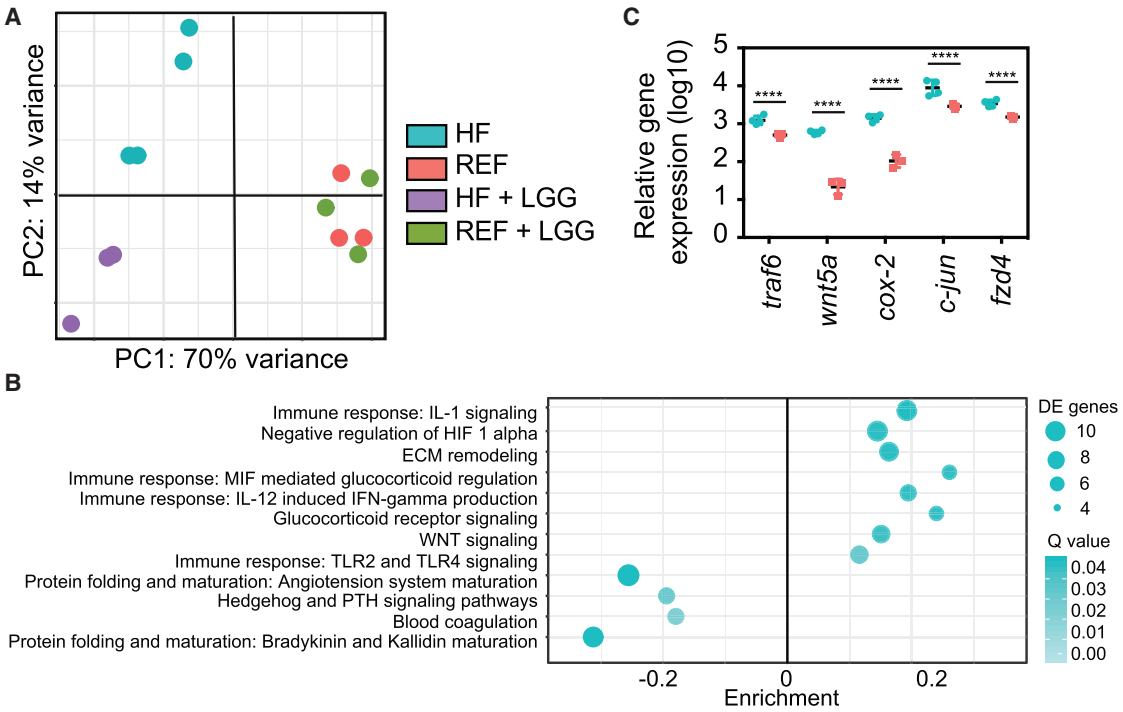

Figure 3. A Simulated HF Regimen Alone Activates Several Oncogenes and Pro-Inflammatory Pathways in Caco-2 Cells

(A) Global expression profiles of Caco-2 cells grown under different conditions. Principal-component analysis (PCA); each dot represents a biological replicate and colors indicate sample type (shown in color key).

(B) Pathway enrichment analysis of Caco-2 cells. Log_2FC of 1 was used as a cut-off. The y axis contains the name of the pathway as provided by MetaCore and shows top enriched pathways based on false discovery rate (FDR). The Q value indicates the significance of the effect on the pathway derived from the p value represented in shades of turquoise. See Tables S2 and S6 for the full list of up- and downregulated pathways. DE, differentially expressed. Data are shown from three REF-exposed and four HF-exposed independent HuMiX experiments.

(C) Relative expression of differentially expressed genes in Caco-2 cells after exposure to the simulated HF regimen or REF medium. Data are shown as mean ± SD for three REF-exposed and four HF-exposed independent HuMiX experiments. Differentially expressed genes were calculated using the Wald test implemented in DESeq2 with Benjamini-Hochberg multiple testing correction at 0.05 significance (Table S2; *p < 0.05; **p < 0.01; ***p < 0.001; ****p < 0.0001). *traf6*, TNF receptor-associated factor-6; *wnt5a*, wingless integrated 5A; *cox-2*, cyclooxygenase-2; *c-jun*, *c-jun* proto-oncogene.

in HF-exposed cells compared with REF-exposed cells (Figures 2C and S2A; Table S1).

A Simulated HF Regimen Alone Activates Several Oncogenes and Pro-inflammatory Pathways in Caco-2 Cells

Next, we evaluated the effect of the simulated HF regimen on Caco-2 cell proliferation and viability. Although growth and viability of Caco-2 cells in HuMiX were comparable between the simulated dietary regimens (Figures S2D and S2E), the regimens had a pronounced effect on the global transcriptome profile of Caco-2 cells (Figure 3A). To place the transcriptome data into biological context and reveal CRC signatures in human cells, we performed a pathway analysis. When exposed to the simulated HF regimen, the most enriched pathways were among others responsible for regulating inflammatory responses in CRC (Figure 3B; Table S2), e.g., IL-1 signaling (Voronov and Apte, 2015; Wang and Dubois, 2010).

The network objects identified from the pathway analysis included the IL-1 receptor 1 (*il-1r1*), as well as its downstream targets, TNF receptor-associated factor (*traf6*), cyclooxygenase-2 (*cox-2*), and *c-jun* (Figure 3C). The wingless integrated (WNT) pathway included such network objects as ligand *wnt5a* as well as downstream targets, such as *snai1* and Frizzled-4 (*fzd4*), which were upregulated only when Caco-2 cells were exposed to the simulated HF regimen (Figure 3C; Table S2). Wnt signaling and its downstream targets are known to be involved in CRC progression and drug resistance (Chikazawa et al., 2010; Guo et al., 2016; Voronov and Apte, 2015; Zhan et al., 2017) and are moderated in part by dietary agents (Tarapore et al., 2012).

A Simulated HF Regimen Affects Gene Expression and Metabolism of a Probiotic

We evaluated the effect of the simulated HF regimen on LGG growth and viability. Although LGG viability was not significantly affected by the presence of HF or REF medium (Figure S2F), LGG growth was significantly reduced in the presence of the simulated HF regimen than with REF (Figure S2G). The simulated dietary regimen had a marked effect on the global transcriptome profile of LGG (Figure 4A), similar to what we observed for the human cells; we observed 355 differentially expressed genes in LGG, including 47 upregulated hypothetical proteins, when exposed to the simulated HF regimen versus the REF medium.

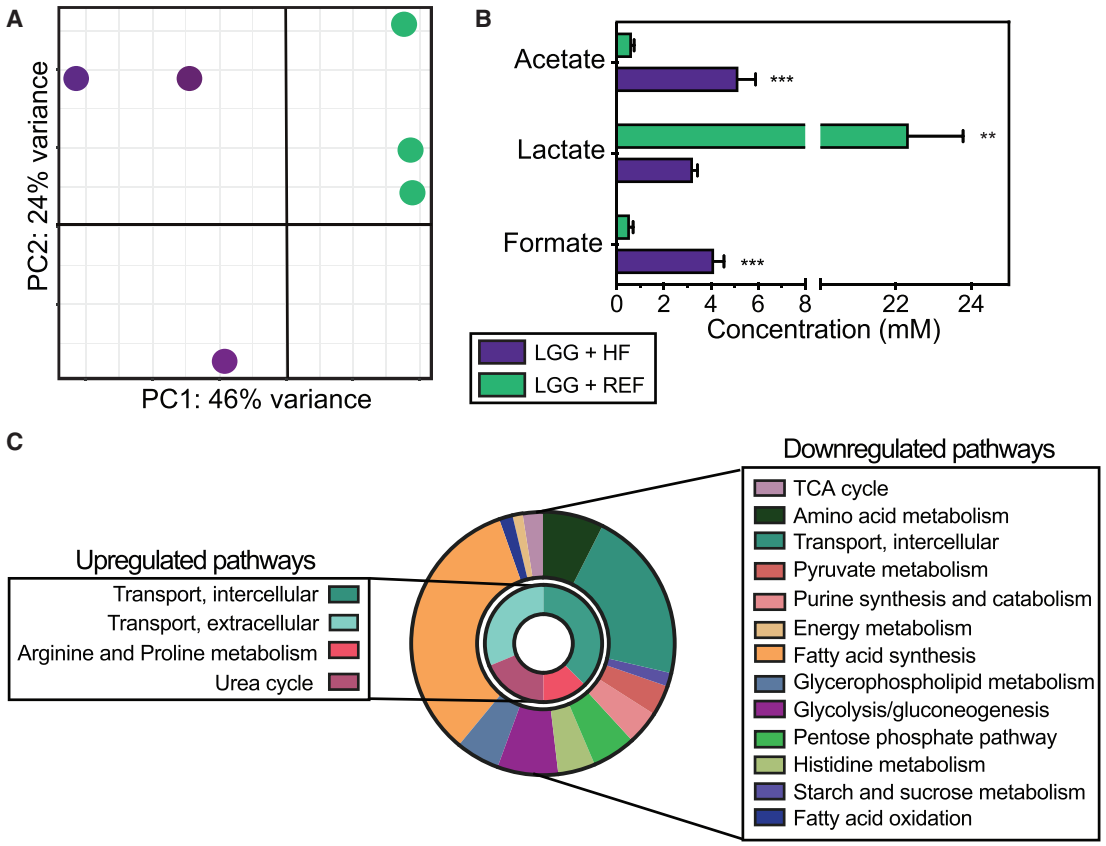

Figure 4. A Simulated HF Regimen Affects Gene Expression and Metabolism of the Probiotic LGG

(A) Global expression profiles of LGG grown under HF or REF dietary regimens and co-culture with Caco-2 cells in HuMiX. PCA; each dot represents a biological replicate and colors indicate sample type (shown in color key).

(B) Measurement of organic and SCFA secretion products by LGG grown in the presence of HF or REF medium. Values are based on technical triplicates and five independent experiments and include background subtraction from fresh medium, normalized to cell count. Statistical significance was calculated using Welch's t test (**$p < 0.01$; ***$p < 0.001$). See also Table S3.

(C) Metabolic pathways with differential flux span in the probiotic LGG when exposed to the simulated HF regimen compared to REF regimen as determined by the *in silico* modeling. The inner ring shows the upregulated pathways; the outer ring shows the downregulated pathways. Each section of the plot indicates the fraction (in %) of total listed pathways.

Genes encoding the cellobiose transporter were upregulated in LGG in the presence of the simulated HF regimen, suggesting the catabolism of prebiotic components by LGG. Indeed, catabolism of prebiotic components used in our simulated HF medium (e.g., arabinogalactan, xylan) has previously been suggested for *Lactobacillus* species (Douillard et al., 2013; Jaskari et al., 1998). These prior observations were supported by our own metabolomic analyses of organic and short-chain fatty acids in the supernatant (spent medium) when LGG is provided with different dietary substrates. For instance, when LGG is provided with simple sugars (REF medium), mainly lactate and smaller amounts of acetate and formate are produced (22.6 mM, 0.76 mM, and 0.52 mM respectively). In stark contrast, less lactate (3.22 mM) but significantly higher levels of acetate (5.15 mM) and formate (4.12 mM) were observed when LGG was grown in the simulated HF medium (Figure 4B; Table S3). *In silico*, 13 subsystems had reactions with decreased flux spans in the LGG metabolic model under the simulated HF regimen compared with the REF medium, including the TCA cycle, amino acid and energy metabolism, glycolysis and gluconeogenesis, and starch and sucrose metabolism, as well as fatty acid oxidation and synthesis (Figure 4C). Four additional subsystem reactions had larger flux spans in LGG under the simulated HF regimen, including the subsystems of transport, arginine and proline metabolism, and the urea cycle (Figure 4C). This indicates that dietary substrates are differentially metabolised by the probiotic LGG and it produces highly diet-dependent combinations of organic acids (e.g., formate and lactate) and SCFAs (e.g., acetate).

Competition and Metabolic Cross-Feeding between the Probiotic and Caco-2 Cells

We further investigated how the different dietary regimens affected the metabolism of the human cells and the probiotic by analyzing the intracellular metabolites of both cell contingents following co-culture in the HuMiX model (Figure 5A; Tables S1, S4, and S5). Although the intracellular concentrations of amino acids such as leucine and glutamine were higher in Caco-2 cells when grown in the presence of the simulated HF regimen in

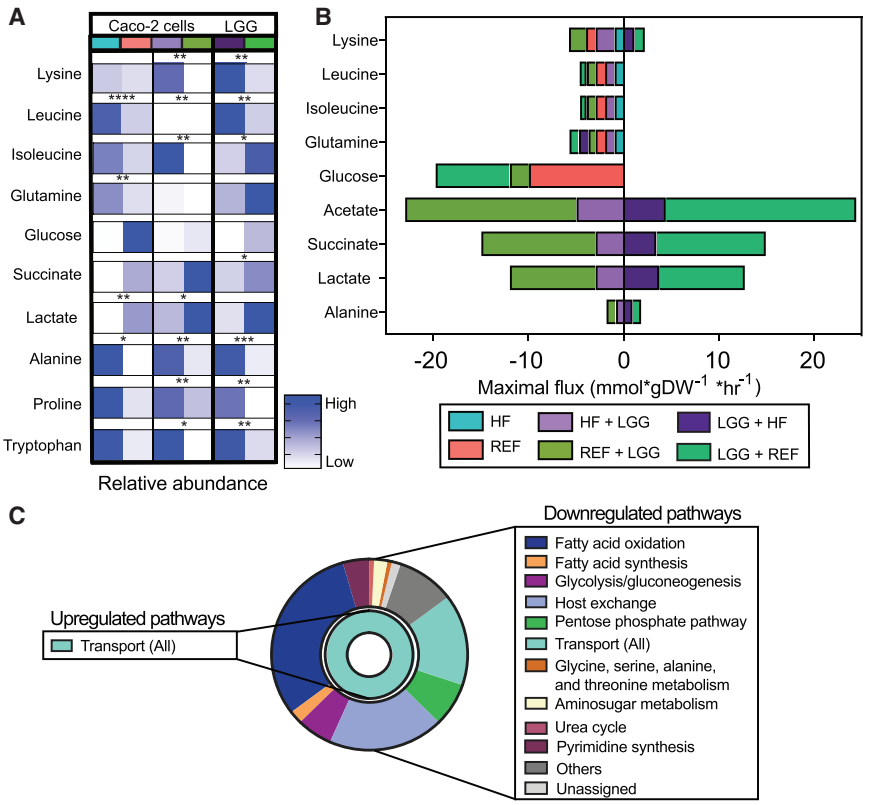

Figure 5. *In Vitro* and *In Silico* Metabolic Changes in Caco-2 Cells and LGG after Co-culture in HuMiX

(A) Relative abundances of *in vitro* intracellular metabolites in Caco-2 cells and LGG. Values are based on technical duplicates and three independent HuMiX experiments. Colors indicate sample type (shown in color key) and stronger shades of blue indicate increased relative abundance. Values compare the effect of the simulated HF regimen versus the REF medium, and to the effect of HF + LGG versus REF + LGG. Statistical significance was calculated using Welch's t test (*$p < 0.05$; **$p < 0.01$; ***$p < 0.001$; ****$p < 0.0001$). See also Figure S2A and Tables S1 and S4.

(B) *In silico* simulation of maximal flux of metabolites in Caco-2 cells and LGG. Negative values indicate consumption of the metabolite, positive values indicate production of the metabolite in mmol per gram dry weight per hour (mmol* g DW^{-1} hr^{-1}). Colors indicate sample type (shown in color key).

(C) Reactions with differential flux span in Caco-2 cells with HF + LGG compared to cells with REF + LGG as determined by the *in silico* modeling. The outer ring shows the fraction (in % of total) of downregulated pathways; the inner ring shows upregulated pathways.

comparison to cells grown in the presence of REF medium, the relative intracellular abundance of these amino acids in Caco-2 cells when co-cultured with the probiotic were significantly lower, regardless of the simulated diet used (Figure 5A; Tables S1 and S5). *In silico,* the flux spans through internal exchange reactions, which reflect nutrient exchange between Caco-2 cells and LGG, showed that both types of cells used these amino acids from the simulated dietary regimens provided, suggesting competition for these nutrients (Figure 5B). *In vitro* measurements showed that relative intracellular concentrations of leucine and glutamine were higher in LGG when compared to Caco-2 cells (Figure 5A; Tables S1, S4, and S5). This indicates that the probiotic outcompetes the host for these amino acids. Similarly, the intracellular glucose concentrations in Caco-2 cells, which were highest when the cells were exposed to the REF medium alone, were significantly lower when Caco-2 cells were grown in the presence of the REF medium and LGG. This finding suggests that LGG was consuming the glucose, and therefore less glucose was available for the Caco-2 cells (Figure 5A). By contrast, intracellular lactate concentrations were the highest in Caco-2 cells when exposed to the probiotic LGG, regardless of the simulated diet used (Figure 5A; Table S5). This finding suggests potential metabolic cross-feeding of lactate produced by the probiotic LGG. *In silico*, metabolic cross-feeding was observed between Caco-2 and LGG. Acetate, succinate, lactate, and alanine were secreted by LGG and consumed by Caco-2 cells only when co-cultured with LGG according to the enlarged flux spans associated with the corresponding exchange reactions (Figure 5B). While overall transport reactions in Caco-2 cells and LGG had larger flux spans when provided with the simulated HF regimen, fluxes through fatty acid synthesis and oxidation, glycolysis and gluconeogenesis, and the urea cycle (among other pathways) were decreased in Caco-2 cells (Figure 5C). Taken together, our *in vitro* metabolite profiles and *in silico* simulations highlight metabolic cross-feeding as well as competition for resources between the probiotic LGG and Caco-2 cells.

To better understand which genes or pathways in LGG (when exposed to the simulated HF regimen) were responsible for the observed changes in gene expression in Caco-2 cells, we linked the Caco-2 *in silico* predicted differential fluxes to the LGG differential gene expression data and observed that the functions of 21 genes in LGG were associated with 34 reactions in the Caco-2 cells (Table S7), indicating diet-dependent effects of LGG metabolism on Caco-2 cell metabolism.

The Synbiotic Regimen Decreases Expression of Pro-carcinogenic Genes and ABC-Transporters in Human Cells

Next, we analyzed how growth in the presence of the LGG probiotic altered gene expression in Caco-2 cells. Principal-component analysis showed that the presence of LGG had an effect on the global transcriptome profile of Caco-2 cells grown in the simulated HF regimen but not when REF medium was used (Figure 3A). A total of 1,771 genes was differentially expressed in Caco-2 cells grown in the simulated HF regimen in the presence of LGG compared with the expression in the same dietary regimen in the absence of LGG. Pathway enrichment analysis

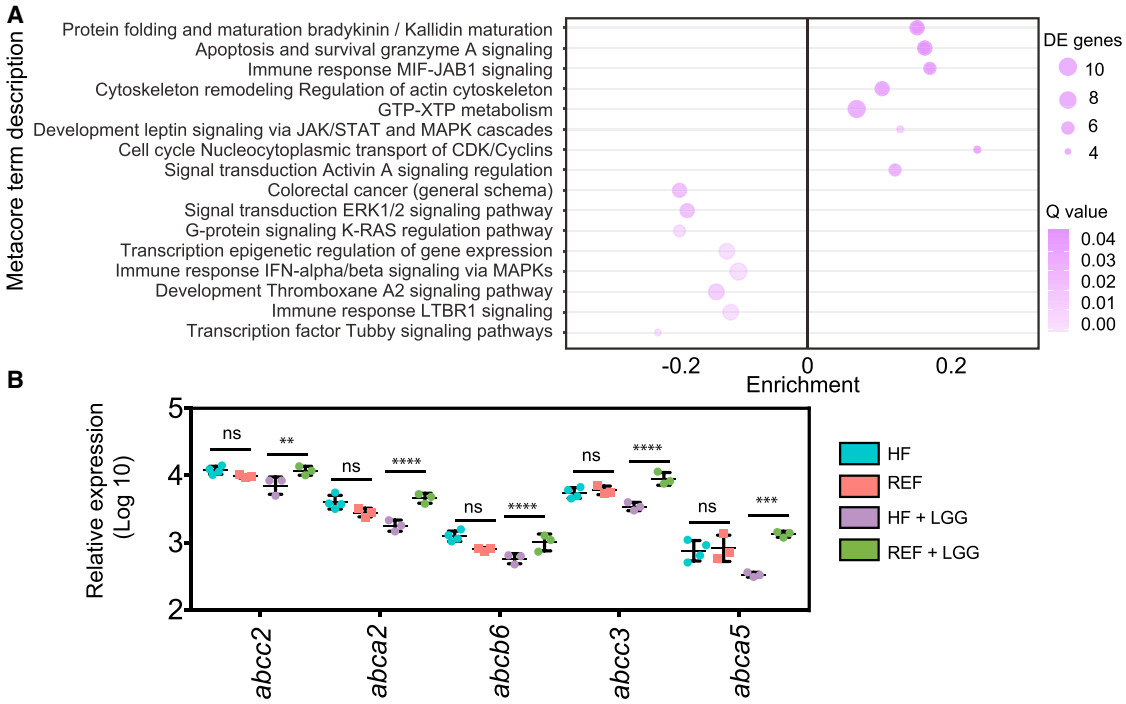

Figure 6. The Synbiotic Regimen Causes Down-Regulation of CRC-Associated Genes and Pathways in Caco-2 Cells

(A) Enrichment pathway analysis of Caco-2 cells when exposed to HF + LGG compared to REF + LGG. Log_2FC of 1 was used as a cut-off. The y axis contains the name of the pathway as provided by MetaCore and shows top enriched pathways based on false discovery rate (FDR). The Q value indicates the significance of the effect on the pathway derived from the p value represented in shades of turquoise. Data are shown from three independent HuMiX experiments per condition. See Tables S2 and S6 for the full list of up- and downregulated pathways, respectively. DE, differentially expressed.

(B) Relative expression of differentially expressed ABC transporter genes in Caco-2 cells. Data are shown as mean ± SD of three independent HuMiX experiments per condition. Colors indicate sample type (shown in color key). Differentially expression analysis was performed using the Wald test implemented in DESeq2 with Benjamini-Hochberg multiple testing correction at 0.05 significance (*p < 0.05; **p < 0.01; ***p < 0.001; ****p < 0.0001). ABC, ATP-binding cassette transporter.

showed that apoptosis and survival granzyme A signaling, as well as protein folding and maturation, were upregulated when Caco-2 cells were exposed to HF + LGG (synbiotic; Figure 6A) but downregulated when exposed to HF alone. Notably, a substantial number of CRC-associated pathways was downregulated including the "colorectal cancer" pathway (as defined in MetaCore), and G-protein *K-RAS* signaling (Figure 6A). Downstream targets of Kirsten rat sarcoma (K-RAS) signaling such as phosphatidylinositol 4,5-bisphosphate 3-kinase catalytic subunit alpha (PI3K-CA) were also downregulated only in the HF + LGG condition (Table S6).

In addition to the downregulated CRC-associated pathways, the expression of several ABC transporters was significantly decreased in Caco-2 cells after co-culture with the combination of HF + LGG (Figure 6B). ABC transporters have been implicated in drug resistance (Gottesman et al., 2002), and high *abcc2* expression has also been associated with the early stages of CRC progression (Andersen et al., 2015). A search of the differentially expressed gene list of Caco-2 cells grown in the presence of HF + LGG against the DrugBank database revealed that the downregulated genes *abcc2*, *abcc3*, *cyp1a1*, *cox-2*, and *cyp2d6* all encode targets of CRC drugs (Table S8). This suggests that probiotics, dietary regimens, and combinations thereof can affect major gene targets of CRC drugs.

The Combination of Organic and Short-Chain Fatty Acids Produced by LGG Is Diet Dependent and Elicits Differential Effects in CRC Cells

The observed changes in host gene expression could be due to the diet-dependent metabolites secreted by LGG (Thomas and Versalovic, 2010). As some of these pathways (e.g., PIK3-CA and the mammalian target of rapamycin [mTOR] signaling pathway) are related to cell self-renewal capacity (Xia and Xu, 2015), we stimulated Caco-2 cells and a primary CRC cell line (T-6) with the fermentation products produced by LGG in the presence of the simulated HF or REF medium. The CRC spheroid cultures were first separately exposed to 10 mM of the individual metabolites (which is between 2.5 and 12.5 times higher than the concentrations of the SCFAs produced by LGG). Under these conditions, the self-renewal capacity significantly increased in both Caco-2 and T-6 cells compared with the untreated controls (Figure 7A). However, when the cells were treated with the respective ratios of metabolites produced by LGG when exposed to the two dietary regimens (Figure 4B), we observed that only the cocktail of molecules reflecting the synbiotic attenuated cancer cell self-renewal capacity (Figures 4B and 7A). Thereby, the distinct, diet-dependent ratios of organic and short-chain fatty acids produced by the probiotic produced during the synbiotic regimen were able to revert

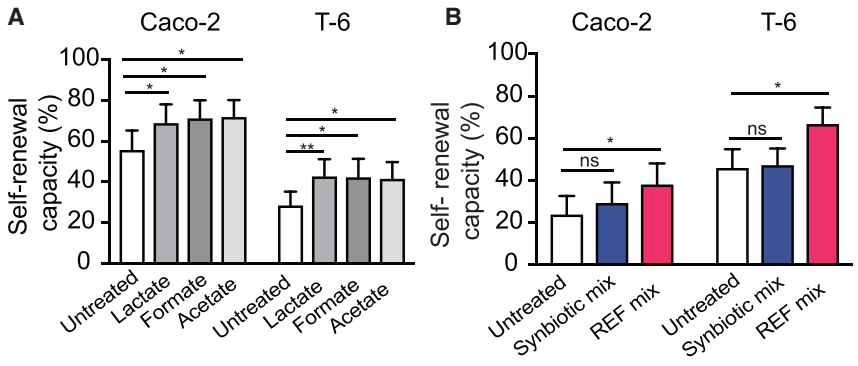

Figure 7. Metabolic Products Produced by LGG under the Different Simulated Dietary Regimens Differentially Impact CRC Cell Growth

Representative assay validated performing three independent experiments using Caco-2 and primary T-6 cells (shown as the mean of technical replicates with 95% confidence interval [CI]).

(A) Effect of individual exposures to acetate, lactate, and formate (10 mM) on CRC cell self-renewal capacity.

(B) Effect of exposure to the diet-dependent cocktail of molecules secreted by LGG on human CRC cells self-renewal capacity. Statistical significance was assessed using a Chi-square test (*$p < 0.05$; **$p < 0.01$). SCFAs, short-chain fatty acids.

the cellular hallmarks of tumor progression and disease dissemination.

DISCUSSION

CRC is a multifactorial disease, and different cellular pathways play a role at different stages. While the combined use of pre- and probiotics may support the treatment of CRC (Ho et al., 2018), limited research exists to explain the mechanisms of action of such synbiotic regimens due to methodological limitations. Therefore, we expanded our HuMiX gut-on-a-chip model to co-culture CRC-derived epithelial cells with a model probiotic under a simulated prebiotic HF regimen. By using our integrated multi-omic approach in combination with *in vitro* and *in silico* metabolic modeling, we were able to unravel the combinatorial effects of the studied synbiotic regimen on CRC cells. Observed effects included downregulation of CRC-associated signaling pathways and drug-resistance genes, and enhanced metabolic competition as well as the production of specific ratios of small molecules which attenuated cancer cell self-renewal capacity.

Inflammatory responses have been linked to both the development and progression of CRC (Rhodes and Campbell, 2002). Exposure of CRC-derived cells to the simulated prebiotic regimen (HF alone) led to an upregulation of signaling pathways related to inflammation. Experimental and clinical studies indicate that colonocyte homeostasis requires gut microbial fermentation of dietary fiber. Oxidative stress and inflammation in the colon can thereby be caused by dysbiotic luminal fermentation and/or deficiencies in SCFAs (Harty, 2013; Singh et al., 2018). In addition to deficiencies in SCFAs, specific components present in the HF regimen (e.g., pectins), which in the absence of LGG are not prone to microbial fermentation, are most likely responsible for the pro-inflammatory effects observed in the human cells (Singh et al., 2018). In contrast, when the CRC-derived cells were treated with the synbiotic combination (HF + LGG), inflammation-driven CRC-associated signaling pathways as well as CRC-oncogenes expression were downregulated. Thus, we speculate that the altered gut microbiome composition arising due to harsh CRC treatments, together with the consumption of dietary fiber may indeed promote CRC progression.

Apart from CRC-oncogenes, we observed that the synbiotic formulation reduced the expression of ATP-binding cassette (ABC) transporter genes, which play roles in the resistance to anti-cancer drugs (Gottesman et al., 2002). In fact, overexpression of these transporters is the most commonly observed mechanism through which cancer cells become drug resistant (Davis and Tew, 2017; Szakács et al., 2006). Therefore, the targeting of ABC transporter expression may be a promising strategy to sensitize drug-resistant cancer cells (Gottesman et al., 2002). In this context, gut microbiota have the potential to interact with ABC transporters (Mercado-Lubo and McCormick, 2010) and, thus, have been suggested as therapeutic agents for CRC (Hlavata et al., 2012). *Abca2*, which was downregulated in the CRC-derived cells only when exposed to the synbiotic regimen, might be of particular interest because the inhibition of ATP-binding cassette transporter-2 (ABCA2) desensitizes resistant cancer cells (Davis and Tew, 2017). The bacterial toxin cycle inhibiting factor (Cif) has been found to selectively reduce *abcc2* transporter expression and has been shown to increase the sensitivity to chemotherapeutic drugs (Patyar et al., 2010; Ye et al., 2008). We did not identify a homolog of Cif in LGG, which suggests that other bacterial molecules or components in the prebiotic medium elicit similar effects.

Taken together, our results demonstrate that only the synbiotic regimen downregulated the expression of genes conferring drug-resistance. When dietary fiber was provided alone to CRC-derived cells, we observed inflammatory signaling pathways to be upregulated, which is in contrast to the beneficial effects previously observed for dietary fiber consumption in CRC prevention (Murphy et al., 2012). However, our results are in line with a recent cohort study conducted by the European Prospective Investigation into Cancer and Nutrition (EPIC), which found that increased intake of dietary fiber was not associated with increased CRC-survival (Ward et al., 2016). Therefore, synbiotics and/or produced molecules may prove efficacious for decreasing CRC-progression by limiting resistance to anti-cancer drugs in the future.

Because one of the drivers of cancer progression is metabolic competition and cross-feeding in the tumor microenvironment (Chang et al., 2015), it is of relevance to understand what dietary components are utilized by probiotics such as LGG or other commensals that may be located in vicinity of the tumor. Regardless of which dietary regimen was provided, the probiotic utilized the same substrates as the host cells *in vitro* and *in silico,* highlighting competition over resources. Furthermore, the flux span analysis of exchange reactions showed that several metabolites

secreted by the probiotic, namely lactate, succinate, alanine, and acetate, were only available to the CRC-derived cells when co-cultured with the probiotic (metabolic cross-feeding). Enteric bacteria interact extensively with the host through metabolic substrate exchange (Nicholson et al., 2005). Pre- and probiotics should therefore be selected such that the metabolic end products of a synbiotic regimen may not promote cancer cell growth. In this context, our results underpin the concept of formulating synbiotic regimens that limit metabolic cross-feeding and enhance competition between the gut microbiome and host cells, thereby limiting the production of primary substrates for CRC cell growth.

We further investigated whether the production of specific molecules secreted by the probiotic under the different simulated regimens may exhibit specific anti-cancer properties. *Lactobacilli* are capable of hydrolyzing dietary fiber (Gänzle and Follador, 2012), but the resulting metabolic end products so far remain elusive. Inconsistencies in human trials concerning probiotic supplementation for CRC patient could be due to highly individualized diet-probiotic combinations. Here, we demonstrate that the probiotic LGG produces a distinct set of metabolites according to available dietary substrates and, consequently, the beneficial effects of probiotic supplementation largely depend on diet. For instance, the molecular cocktail produced by LGG during the synbiotic regimen attenuated cancer cell self-renewal capacity. Self-renewal capacity is a proxy for a cell's ability to maintain an undifferentiated state and to form colonies (Francipane and Lagasse, 2014; He et al., 2009). This in turn depends on the function of cellular and molecular pathway(s) essential for the growth and the maintenance of self-renewal of cancer stem cells (e.g., the PIK3-CA and mTOR signaling pathway) (Xia and Xu, 2015). It has not escaped our attention that the downregulation of this pathway in the CRC-derived cells might be due to the diet-dependent cocktail of molecules produced by the probiotic.

Our results demonstrate the importance of including dietary formulations, such as the synbiotic combination tested here, into CRC treatment plans (Niero et al., 2014). Further studies, including investigations of additional combinations of synbiotics, are necessary to further explore the mechanisms through which prebiotics and probiotics influence the molecular and cellular hallmarks of CRC cells. Of particular interest will be studies that use different synbiotic regimens as adjuvants, i.e., in combination with anti-cancer drug treatments. In this context, our findings may also be of interest for the treatment of inflammatory diseases of the gut that may precede CRC, such as inflammatory bowel disease. Additional studies involving representative, complex gut microbiota will also be required to understand the physiological repercussions of synbiotics in relation to the overall microbial context of the human gut. Finally, personalized *in vitro* models comprising primary CRC-derived cells and the microbiota from the same individual will allow to delineate individual-specific responses to formulate personalized treatment regimens. The combination of *in vitro* models, such as HuMiX, with *in silico* simulations will, thus, prove indispensable to unravel the combinatorial effects of synbiotics and drugs for improved anti-cancer treatments in the future.

STAR★METHODS

Detailed methods are provided in the online version of this paper and include the following:

- KEY RESOURCES TABLE
- CONTACT FOR REAGENT AND RESOURCE SHARING
- EXPERIMENTAL MODEL AND SUBJECT DETAILS
  - Human Cell Culture
  - Primary cell culture
  - Bacterial cell culture
- METHOD DETAILS
  - The HuMiX model
  - Biomacromolecular extraction
  - Intracellular metabolite extraction
  - Cell viability and counting
  - SCFAs extraction
  - SCFAs measurement
  - Lactate measurement
  - RNA library preparation for Caco-2 and LGG
  - Simulated media preparation
  - Sphere and 3D colony formation assays
  - qRT-PCR validation
  - *In silico* model predictions
  - *In silico* diet-host-bacteria reconstruction
  - Drug target identification
- QUANTIFICATION AND STATISTICAL ANALYSIS
  - Intracellular metabolomics analysis
  - SCFA quantification
  - *In silico* analysis
  - RNA-sequencing analysis
  - Differential expression analysis
  - Pathway enrichment analysis
- DATA AND SOFTWARE AVAILABILITY

SUPPLEMENTAL INFORMATION

Supplemental Information can be found online at https://doi.org/10.1016/j.celrep.2019.04.001.

ACKNOWLEDGMENTS

The authors would like to thank Dr. Christian Jäger at the LCSB Metabolomics Platform for helpful discussions and metabolite quantification, and Martine Schmitz for RT-PCR validation analysis. We thank the contributing surgeons from the Centre Hospitalier Emile Mayrisch in Esch-sur-Alzette and the nurses of the Clinical and Epidemiological Investigation Center of the Luxembourg Institute of Health for collecting samples for research purposes. The authors wish to thank Frutarom for providing the SoyLife prebiotic. K.G. was supported by an AFR PhD fellowship from the Luxembourg National Research Fund (FNR; AFR/PHD/9964547). This work was supported by a Luxembourg Personalised Medicine Consortium pump-prime grant (PerPreProBioCRC) and a proof-of-concept grant (PoC/15/11014639) from the FNR, awarded to P.W. The project was also supported through an internal research project grant (IRP; MiDiCa) from the University of Luxembourg to S.H. and P.W., and two CORE Junior grants (C14/BM/8066232 and C16/BM/11282028) awarded to J.F. and E.L., respectively. This work was further supported by an ATTRACT Programme grant (FNR/A12/01) awarded to I.T., a European Research Council (ERC) grant under the European Union's Horizon 2020 research and innovation programme (grant agreement No. 757922) awarded to I.T., and an FNR grant (PRIDE15/10675146/CANBIO) to T.B.

AUTHOR CONTRIBUTIONS

Conceptualization, K.G., E.L., S.H., and P.W.; Methodology, K.G., E.L., S.H., and P.W.; Formal Analysis, K.G., J.R.G., and A.H.; Investigation, K.G., J.B., A.F., J.V.F., P.S., and P.U.; Writing – Original Draft, P.W. and K.G.; Writing – Review & Editing, J.R.G., A.H., M.P.P., T.B., P.U., J.B., A.F., R.H., J.V.F., E.L., T.S., I.T., and S.H.; Funding Acquisition, K.G., E.L., J.F., T.B., S.H., I.T., T.S., and P.W.; Supervision E.L., J.V.F., J.B., T.S, S.H., I.T., and P.W.

DECLARATION OF INTERESTS

The authors P.W. and K.G. have a corresponding patent application (EP18206858), which is currently pending.

Received: October 29, 2018
Revised: February 11, 2019
Accepted: March 28, 2019
Published: April 30, 2019

REFERENCES

Altman, B.J., Stine, Z.E., and Dang, C.V. (2016). From Krebs to clinic: glutamine metabolism to cancer therapy. Nat. Rev. Cancer *16*, 619–634.

Anders, S., and Huber, W. (2010). Differential expression analysis for sequence count data. Genome Biol. *11*, R106.

Andersen, V., Vogel, L.K., Kopp, T.I., Sæbø, M., Nonboe, A.W., Hamfjord, J., Kure, E.H., and Vogel, U. (2015). High ABCC2 and low ABCG2 gene expression are early events in the colorectal adenoma-carcinoma sequence. PLoS ONE *10*, e0119255.

Armaghany, T., Wilson, J.D., Chu, Q., and Mills, G. (2012). Genetic alterations in colorectal cancer. Gastrointest. Cancer Res. *5*, 19–27.

Baldini, F., Heinken, A., Heirendt, L., Magnusdottir, S., Fleming, R.M.T., and Thiele, I. (2018). The Microbiome Modeling Toolbox: from microbial interactions to personalized microbial communities. Bioinformatics, Published online November 21, 2018. https://doi.org/10.1093/bioinformatics/bty941.

Bein, A., Shin, W., Jalili-Firoozinezhad, S., Park, M.H., Sontheimer-Phelps, A., Tovaglieri, A., Chalkiadaki, A., Kim, H.J., and Ingber, D.E. (2018). Microfluidic Organ-on-a-Chip Models of Human Intestine. Cell. Mol. Gastroenterol. Hepatol. *5*, 659–668.

Blot, W.J., and Tarone, R.E. (2015). Doll and Peto's quantitative estimates of cancer risks: holding generally true for 35 years. J. Natl. Cancer Inst. *107*, djv044.

Caccialanza, R., Pedrazzoli, P., Cereda, E., Gavazzi, C., Pinto, C., Paccagnella, A., Beretta, G.D., Nardi, M., Laviano, A., and Zagonel, V. (2016). Nutritional Support in Cancer Patients: A Position Paper from the Italian Society of Medical Oncology (AIOM) and the Italian Society of Artificial Nutrition and Metabolism (SINPE). J. Cancer *7*, 131–135.

Chang, C.H., Qiu, J., O'Sullivan, D., Buck, M.D., Noguchi, T., Curtis, J.D., Chen, Q., Gindin, M., Gubin, M.M., van der Windt, G.J.W., et al. (2015). Metabolic competition in the tumor microenvironment is a driver of cancer progression. Cell *162*, 1229–1241.

Chikazawa, N., Tanaka, H., Tasaka, T., Nakamura, M., Tanaka, M., Onishi, H., and Katano, M. (2010). Inhibition of Wnt signaling pathway decreases chemotherapy-resistant side-population colon cancer cells. Anticancer Res. *30*, 2041–2048.

Corrado, M., Scorrano, L., and Campello, S. (2016). Changing perspective on oncometabolites: from metabolic signature of cancer to tumorigenic and immunosuppressive agents. Oncotarget *7*, 46692–46706.

Davis, W., Jr., and Tew, K.D. (2017). ATP-binding cassette transporter-2 (ABCA2) as a therapeutic target. Biochem Pharmacol *151*, 188–200.

DiMarco-Crook, C., and Xiao, H. (2015). Diet-based strategies for cancer chemoprevention: the role of combination regimens using dietary bioactive components. Annu. Rev. Food Sci. Technol. *6*, 505–526.

Dobin, A., Davis, C.A., Schlesinger, F., Drenkow, J., Zaleski, C., Jha, S., Batut, P., Chaisson, M., and Gingeras, T.R. (2013). STAR: ultrafast universal RNA-seq aligner. Bioinformatics *29*, 15–21.

Douillard, F.P., Ribbera, A., Järvinen, H.M., Kant, R., Pietilä, T.E., Randazzo, C., Paulin, L., Laine, P.K., Caggia, C., von Ossowski, I., et al. (2013). Comparative genomic and functional analysis of Lactobacillus casei and Lactobacillus rhamnosus strains marketed as probiotics. Appl. Environ. Microbiol. *79*, 1923–1933.

FAO, and WHO. (2002). Guidelines for evaluation of probiotics in food. Report of a Joint FAO/WHO Working Group on Drafting Guidelines for the Evaluation of Probiotics in Food,, Food and Agriculture Organization of United Nations and World Health Organization, April 30 and May 1, 2002. https://www.who.int/foodsafety/fs_management/en/probiotic_guidelines.pdf.

Francipane, M.G., and Lagasse, E. (2014). mTOR pathway in colorectal cancer: an update. Oncotarget *5*, 49–66.

Fritz, J.V., Desai, M.S., Shah, P., Schneider, J.G., and Wilmes, P. (2013). From meta-omics to causality: experimental models for human microbiome research. Microbiome *1*, 14.

Gänzle, M.G., and Follador, R. (2012). Metabolism of oligosaccharides and starch in lactobacilli: a review. Front. Microbiol. *3*, 340.

Gibson, G.R., Cummings, J.H., and Macfarlane, G.T. (1988). Use of a three-stage continuous culture system to study the effect of mucin on dissimilatory sulfate reduction and methanogenesis by mixed populations of human gut bacteria. Appl. Environ. Microbiol. *54*, 2750–2755.

Gottesman, M.M., Fojo, T., and Bates, S.E. (2002). Multidrug resistance in cancer: role of ATP-dependent transporters. Nat. Rev. Cancer *2*, 48–58.

Gudmundsson, S., and Thiele, I. (2010). Computationally efficient flux variability analysis. BMC Bioinformatics *11*, 489.

Guo, B., Fu, S., Zhang, J., Liu, B., and Li, Z. (2016). Targeting inflammasome/IL-1 pathways for cancer immunotherapy. Sci. Rep. *6*, 36107.

Harty, R.F. (2013). Energy, oxidative stress, and inflammation in the colon. Dig. Dis. Sci. *58*, 3386–3388.

He, S., Nakada, D., and Morrison, S.J. (2009). Mechanisms of stem cell self-renewal. Annu. Rev. Cell Dev. Biol. *25*, 377–406.

Heinken, A., Sahoo, S., Fleming, R.M., and Thiele, I. (2013). Systems-level characterization of a host-microbe metabolic symbiosis in the mammalian gut. Gut Microbes *4*, 28–40.

Heirendt, L., Arreckx, S., Pfau, T., Mendoza, S.N., Richelle, A., Heinken, A., Haraldsdóttir, H.S., Wachowiak, J., Keating, S.M., Vlasov, V., et al. (2019). Creation and analysis of biochemical constraint-based models using the COBRA Toolbox v.3.0. Nat. Protoc. *14*, 639–702.

Hildebrand, F., Nguyen, T.L., Brinkman, B., Yunta, R.G., Cauwe, B., Vandenabeele, P., Liston, A., and Raes, J. (2013). Inflammation-associated enterotypes, host genotype, cage and inter-individual effects drive gut microbiota variation in common laboratory mice. Genome Biol. *14*, R4.

Hiller, K., Hangebrauk, J., Jäger, C., Spura, J., Schreiber, K., and Schomburg, D. (2009). MetaboliteDetector: comprehensive analysis tool for targeted and nontargeted GC/MS based metabolome analysis. Anal. Chem. *81*, 3429–3439.

Hlavata, I., Mohelnikova-Duchonova, B., Vaclavikova, R., Liska, V., Pitule, P., Novak, P., Bruha, J., Vycital, O., Holubec, L., Treska, V., et al. (2012). The role of ABC transporters in progression and clinical outcome of colorectal cancer. Mutagenesis *27*, 187–196.

Ho, C.L., Tan, H.Q., Chua, K.J., Kang, A., Lim, K.H., Ling, K.L., Yew, W.S., Lee, Y.S., Thiery, J.P., and Chang, M.W. (2018). Engineered commensal microbes for diet-mediated colorectal-cancer chemoprevention. Nat. Biomed. Eng. *2*, 27–37.

Hu, Y., and Smyth, G.K. (2009). ELDA: extreme limiting dilution analysis for comparing depleted and enriched populations in stem cell and other assays. J. Immunol. Methods *347*, 70–78.

Huerta-Cepas, J., Forslund, K., Coelho, L.P., Szklarczyk, D., Jensen, L.J., von Mering, C., and Bork, P. (2017). Fast Genome-Wide Functional Annotation

through Orthology Assignment by eggNOG-Mapper. Mol. Biol. Evol. *34*, 2115–2122.

Hutkins, R.W., Krumbeck, J.A., Bindels, L.B., Cani, P.D., Fahey, G., Jr., Goh, Y.J., Hamaker, B., Martens, E.C., Mills, D.A., Rastal, R.A., et al. (2016). Prebiotics: why definitions matter. Curr. Opin. Biotechnol. *37*, 1–7.

Jang, M., Kim, S.S., and Lee, J. (2013). Cancer cell metabolism: implications for therapeutic targets. Exp. Mol. Med. *45*, e45.

Jaskari, J., Kontula, P., Siitonen, A., Jousimies-Somer, H., Mattila-Sandholm, T., and Poutanen, K. (1998). Oat beta-glucan and xylan hydrolysates as selective substrates for Bifidobacterium and Lactobacillus strains. Appl. Microbiol. Biotechnol. *49*, 175–181.

Kim, N.H., Cha, Y.H., Lee, J., Lee, S.H., Yang, J.H., Yun, J.S., Cho, E.S., Zhang, X., Nam, M., Kim, N., et al. (2017). Snail reprograms glucose metabolism by repressing phosphofructokinase PFKP allowing cancer cell survival under metabolic stress. Nat. Commun. *8*, 14374.

Kogel, K.H., Voll, L.M., Schäfer, P., Jansen, C., Wu, Y., Langen, G., Imani, J., Hofmann, J., Schmiedl, A., Sonnewald, S., et al. (2010). Transcriptome and metabolome profiling of field-grown transgenic barley lack induced differences but show cultivar-specific variances. Proc. Natl. Acad. Sci. USA *107*, 6198–6203.

Koh, A., De Vadder, F., Kovatcheva-Datchary, P., and Bäckhed, F. (2016). From Dietary Fiber to Host Physiology: Short-Chain Fatty Acids as Key Bacterial Metabolites. Cell *165*, 1332–1345.

Kopylova, E., Noé, L., and Touzet, H. (2012). SortMeRNA: fast and accurate filtering of ribosomal RNAs in metatranscriptomic data. Bioinformatics *28*, 3211–3217.

Langmead, B., and Salzberg, S.L. (2012). Fast gapped-read alignment with Bowtie 2. Nat. Methods *9*, 357–359.

Le Leu, R.K., Brown, I.L., Hu, Y., Bird, A.R., Jackson, M., Esterman, A., and Young, G.P. (2005). A synbiotic combination of resistant starch and Bifidobacterium lactis facilitates apoptotic deletion of carcinogen-damaged cells in rat colon. J. Nutr. *135*, 996–1001.

Liao, Y., Smyth, G.K., and Shi, W. (2014). featureCounts: an efficient general purpose program for assigning sequence reads to genomic features. Bioinformatics *30*, 923–930.

Magnúsdóttir, S., and Thiele, I. (2018). Modeling metabolism of the human gut microbiome. Curr. Opin. Biotechnol. *51*, 90–96.

Magnúsdóttir, S., Heinken, A., Kutt, L., Ravcheev, D.A., Bauer, E., Noronha, A., Greenhalgh, K., Jäger, C., Baginska, J., Wilmes, P., et al. (2017). Generation of genome-scale metabolic reconstructions for 773 members of the human gut microbiota. Nat. Biotechnol. *35*, 81–89.

Mercado-Lubo, R., and McCormick, B.A. (2010). The interaction of gut microbes with host ABC transporters. Gut Microbes *1*, 301–306.

Moreau, N.M., Goupry, S.M., Antignac, J.P., Monteau, F.J., Le Bizec, B.J., Champ, M.M., Martin, L.J., and Dumon, H.J. (2003). Simultaneous measurement of plasma concentrations and 13C-enrichment of short-chain fatty acids, lactic acid and ketone bodies by gas chromatography coupled to mass spectrometry. J. Chromatogr. B Analyt. Technol. Biomed. Life Sci. *784*, 395–403.

Morin, A., Letouzé, E., Gimenez-Roqueplo, A.P., and Favier, J. (2014). Oncometabolites-driven tumorigenesis: From genetics to targeted therapy. Int. J. Cancer *135*, 2237–2248.

Murphy, N., Norat, T., Ferrari, P., Jenab, M., Bueno-de-Mesquita, B., Skeie, G., Dahm, C.C., Overvad, K., Olsen, A., Tjønneland, A., et al. (2012). Dietary fibre intake and risks of cancers of the colon and rectum in the European prospective investigation into cancer and nutrition (EPIC). PLoS ONE *7*, e39361.

Nicholson, J.K., Holmes, E., and Wilson, I.D. (2005). Gut microorganisms, mammalian metabolism and personalized health care. Nat. Rev. Microbiol. *3*, 431–438.

Niero, E.L., Rocha-Sales, B., Lauand, C., Cortez, B.A., de Souza, M.M., Rezende-Teixeira, P., Urabayashi, M.S., Martens, A.A., Neves, J.H., and Machado-Santelli, G.M. (2014). The multiple facets of drug resistance: one history, different approaches. J. Exp. Clin. Cancer Res. *33*, 37.

Noronha, A., Modamio, J., Jarosz, Y., Guerard, E., Sompairac, N., Preciat, G., Daníelsdóttir, A.D., Krecke, M., Merten, D., Haraldsdóttir, H.S., et al. (2019). The Virtual Metabolic Human database: integrating human and gut microbiome metabolism with nutrition and disease. Nucleic Acids Res. *47* (*D1*), D614–D624.

Orth, J.D., Thiele, I., and Palsson, B.O. (2010). What is flux balance analysis? Nat. Biotechnol. *28*, 245–248.

Pacheco, M.P., John, E., Kaoma, T., Heinäniemi, M., Nicot, N., Vallar, L., Bueb, J.L., Sinkkonen, L., and Sauter, T. (2015). Integrated metabolic modelling reveals cell-type specific epigenetic control points of the macrophage metabolic network. BMC Genomics *16*, 809.

Patyar, S., Joshi, R., Byrav, D.S.P., Prakash, A., Medhi, B., and Das, B.K. (2010). Bacteria in cancer therapy: a novel experimental strategy. J. Biomed. Sci. *17*, 21.

Paul, W., Marta, C., and Tom, V.W. (2018). Resolving host-microbe interactions in the gut: the promise of in vitro models to complement in vivo research. Curr. Opin. Microbiol. *44*, 28–33.

Pflughoeft, K.J., and Versalovic, J. (2012). Human microbiome in health and disease. Annu. Rev. Pathol. *7*, 99–122.

Qureshi-Baig, K., Ullmann, P., Rodriguez, F., Frasquilho, S., Nazarov, P.V., Haan, S., and Letellier, E. (2016). What Do We Learn from Spheroid Culture Systems? Insights from Tumorspheres Derived from Primary Colon Cancer Tissue. PLoS ONE *11*, e0146052.

Rafter, J., Bennett, M., Caderni, G., Clune, Y., Hughes, R., Karlsson, P.C., Klinder, A., O'Riordan, M., O'Sullivan, G.C., Pool-Zobel, B., et al. (2007). Dietary synbiotics reduce cancer risk factors in polypectomized and colon cancer patients. Am. J. Clin. Nutr. *85*, 488–496.

Rahman, M., Jackson, L.K., Johnson, W.E., Li, D.Y., Bild, A.H., and Piccolo, S.R. (2015). Alternative preprocessing of RNA-Sequencing data in The Cancer Genome Atlas leads to improved analysis results. Bioinformatics *31*, 3666–3672.

Raman, M., Ambalam, P., Kondepudi, K.K., Pithva, S., Kothari, C., Patel, A.T., Purama, R.K., Dave, J.M., and Vyas, B.R. (2013). Potential of probiotics, prebiotics and synbiotics for management of colorectal cancer. Gut Microbes *4*, 181–192.

Read, M.N., and Holmes, A.J. (2017). Towards an Integrative Understanding of Diet-Host-Gut Microbiome Interactions. Front. Immunol. *8*, 538.

Rhodes, J.M., and Campbell, B.J. (2002). Inflammation and colorectal cancer: IBD-associated and sporadic cancer compared. Trends Mol. Med. *8*, 10–16.

Rosenow, C., Saxena, R.M., and Durst, M. (2001). Prokaryotic RNA preparation methods useful for high density array analysis: comparison of two approaches. Nucleic Acids Res. *29*, e112.

Rothenberg, R. (2015). The causes of cancer, revisited. Ann. Epidemiol. *25*, 215–216.

Roume, H., Heintz-Buschart, A., Muller, E.E., and Wilmes, P. (2013). Sequential isolation of metabolites, RNA, DNA, and proteins from the same unique sample. Methods Enzymol. *531*, 219–236.

Ruxton, G.D. (2006). The unequal variance t-test is an underused alternative to Student's t-test and the Mann–Whitney U test. Behav. Ecol. *17*, 688–690.

Scott, M., Gunderson, C.W., Mateescu, E.M., Zhang, Z., and Hwa, T. (2010). Interdependence of cell growth and gene expression: origins and consequences. Science *330*, 1099–1102.

Shah, P., Fritz, J.V., Glaab, E., Desai, M.S., Greenhalgh, K., Frachet, A., Niegowska, M., Estes, M., Jäger, C., Seguin-Devaux, C., et al. (2016). A microfluidics-based in vitro model of the gastrointestinal human-microbe interface. Nat. Commun. *7*, 11535.

Sharma, M., and Shukla, G. (2016). Metabiotics: One Step ahead of Probiotics; an Insight into Mechanisms Involved in Anticancerous Effect in Colorectal Cancer. Front. Microbiol. *7*, 1940.

Singh, V., Yeoh, B.S., Chassaing, B., Xiao, X., Saha, P., Aguilera Olvera, R., Lapek, J.D., Jr., Zhang, L., Wang, W.B., Hao, S., et al. (2018). Dysregulated

Microbial Fermentation of Soluble Fiber Induces Cholestatic Liver Cancer. Cell *175*, 679–694.e22.

Song, M., Wu, K., Meyerhardt, J.A., Ogino, S., Wang, M., Fuchs, C.S., Giovannucci, E.L., and Chan, A.T. (2018). Fiber Intake and Survival After Colorectal Cancer Diagnosis. JAMA Oncol. *4*, 71–79.

Szakács, G., Paterson, J.K., Ludwig, J.A., Booth-Genthe, C., and Gottesman, M.M. (2006). Targeting multidrug resistance in cancer. Nat. Rev. Drug Discov. *5*, 219–234.

Tarapore, R.S., Siddiqui, I.A., and Mukhtar, H. (2012). Modulation of Wnt/β-catenin signaling pathway by bioactive food components. Carcinogenesis *33*, 483–491.

R Core Team (2016). R: A language and environment for statistical computing (R Foundation for Statistical Computing). https://www.R-project.org/.

R Core Team (2017). R: A language and environment for statistical computing. (R Foundation for Statistical Computing).

Tenenbaum, D. 2017. KEGGREST: Client-side REST access to KEGG. R package version 1.16.1.

Theriot, C.M., Koenigsknecht, M.J., Carlson, P.E., Jr., Hatton, G.E., Nelson, A.M., Li, B., Huffnagle, G.B., Li, J.Z., and Young, V.B. (2014). Antibiotic-induced shifts in the mouse gut microbiome and metabolome increase susceptibility to Clostridium difficile infection. Nat. Commun. *5*, 3114.

Thiele, I., Swainston, N., Fleming, R.M., Hoppe, A., Sahoo, S., Aurich, M.K., Haraldsdottir, H., Mo, M.L., Rolfsson, O., Stobbe, M.D., et al. (2013). A community-driven global reconstruction of human metabolism. Nat. Biotechnol. *31*, 419–425.

Thomas, C.M., and Versalovic, J. (2010). Probiotics-host communication: Modulation of signaling pathways in the intestine. Gut Microbes *1*, 148–163.

Valencia, P.M., Richard, M., Brock, J., and Boglioli, E. (2017). The human microbiome: opportunity or hype? Nat. Rev. Drug Discov. *16*, 823–824.

Vlassis, N., Pacheco, M.P., and Sauter, T. (2014). Fast reconstruction of compact context-specific metabolic network models. PLoS Comput. Biol. *10*, e1003424.

Voronov, E., and Apte, R.N. (2015). IL-1 in Colon Inflammation, Colon Carcinogenesis and Invasiveness of Colon Cancer. Cancer Microenviron. *8*, 187–200.

Wang, D., and Dubois, R.N. (2010). The role of COX-2 in intestinal inflammation and colorectal cancer. Oncogene *29*, 781–788.

Ward, H.A., Norat, T., Overvad, K., Dahm, C.C., Bueno-de-Mesquita, H.B., Jenab, M., Fedirko, V., van Duijnhoven, F.J., Skeie, G., Romaguera-Bosch, D., et al. (2016). Pre-diagnostic meat and fibre intakes in relation to colorectal cancer survival in the European Prospective Investigation into Cancer and Nutrition. Br. J. Nutr. *116*, 316–325.

Xia, P., and Xu, X.Y. (2015). PI3K/Akt/mTOR signaling pathway in cancer stem cells: from basic research to clinical application. Am. J. Cancer Res. *5*, 1602–1609.

Ye, S., MacEachran, D.P., Hamilton, J.W., O'Toole, G.A., and Stanton, B.A. (2008). Chemotoxicity of doxorubicin and surface expression of P-glycoprotein (MDR1) is regulated by the Pseudomonas aeruginosa toxin Cif. Am. J. Physiol. Cell Physiol. *295*, C807–C818.

Young, M., Ordonez, L., and Clarke, A.R. (2013). What are the best routes to effectively model human colorectal cancer? Mol. Oncol. *7*, 178–189.

Zhan, T., Rindtorff, N., and Boutros, M. (2017). Wnt signaling in cancer. Oncogene *36*, 1461–1473.

STAR★METHODS

KEY RESOURCES TABLE

REAGENT or RESOURCE	SOURCE	IDENTIFIER
Biological samples		
T6 Cells from primary CRC tissue (male)	IBBL	Reference 201009/09
Chemicals, Peptides, and Recombinant Proteins		
Bactopeptone	BD Biosciences	Cat #211677
Starch, from potato	Sigma-Aldrich	Cat #33615
Xylan, from beechwood	Sigma-Aldrich	Cat #X4252
(+) - Arabinogalactan, from larch wood	Sigma-Aldrich	Cat #10830
Amylopectin, from maize	Sigma-Aldrich	Cat #10120
Pectin, from apple	Sigma-Aldrich	Cat #76282
Casein Hydrosylate	Sigma-Aldrich	Cat #22090
Ox-bile, dehydrated, purified	Sigma-Aldrich	Cat #70168
SoyLife®	https://www.soylife.com/	Frutarom
Menadione	Sigma-Aldrich	Cat #M57405
Hydrogen Chloride, HCl	Sigma-Aldrich	Cat #295426
Cysteine	Sigma-Aldrich	C7352
Dimethyl sulfoxide, DMSO	Sigma- Aldrich	D2650
Trace Mineral Supplement	ATCC	ATCC®MD-TMS
Brain Heart Infusion Broth, BHIB	Sigma-Aldrich	Cat #53286
Hemin	Sigma-Aldrich	Cat #51280
Dulbecco's Modified Eagle's Medium, DMEM (high glucose)	Sigma-Aldrich	Cat #D6429
Foetal Bovine Serum, FBS	ThermoFisher	Cat #10500-064 (Lot: 1096628)
Vitamin Supplement	ATCC	ATCC®MD-VS
Dulbecco's- Phosphate–Buffered Saline, D-PBS	Sigma-Aldrich	Cat #14190-169
Trypsin	Sigma-Aldrich	Cat #T3924
Collagen	Invitrogen	Cat #A1048301
Mucin, from porcine stomach	Sigma-Aldrich	M1778
Methylcellulose-based media MethoCult	STEMCELL Technologies	H4100
Epidermal Growth Factor, EGF	Biomol	Ref 50349.500
Formaldehyde solution 37%	Carl Roth	Ref 4979.1
Basic Fibroblast Growth Factor, bFGF	Miltenyi Biotec	Ref 130-093-841
DMEM-F12	Westburg	Ref BE12-719F/12
B27	ThermoFisher	Ref 12587-010
Insulin	Sigma-Aldrich	Ref I9278
Glucose	Sigma-Aldrich	G8769
Heparin	Sigma-Aldrich	H3149-50KU
1% Penicillin/Streptomycin (P/S)	Lonza	17-602E
Bacteria counting beads	ThermoFisher	C#36950
Precelly's Glass beads (0.15-0.2 mm)	Sigma-Aldrich	Ref G1145
Chloroform	Merck	Ref 102444
Methanol hypergrade for LC-MS	Merck	Ref 106035
2- Ethylbutyric acid	Sigma-Aldrich	109959
Hydrochloric acid 37%	Sigma Aldrich	320331
Diethyl ether	VWR	1.00921.1000

(*Continued on next page*)

Continued

REAGENT or RESOURCE	SOURCE	IDENTIFIER
Methoxyamine Hydrochloride	Sigma-Aldrich	226904
N-methyl-N-trimethylsilyl-trifluoroacetamide (MTBSTFA)	Macherey-Nagel (Interscience)	89035610
Volatile free acid mix analytical standard	Sigma-Aldrich	CRM46975
Critical Commercial Assays		
Live/Dead Fixable Near-IR Dead Cell Stain Kit	ThermoFisher	L10119
Live-dead Bac Light bacterial viability Kit	Life Technologies	Cat #L7012
AllPrep DNA/RNA/Protein Kit	QIAGEN	Cat # 80004
All-in-One-Norgen Purification kit	Norgen	Cat #1024200
NEBNext Ultra Directional RNA Library Prep Kit for Illumina	New England Biolabs	Cat #E7420
Ribo-Zero rRNA Removal Kit (bacteria)	Illumina	MRZB12424
SYBR Green Supermix	Biorad	Ref 170-8885
SuperScript ^{TM} III First-Strand Synthesis System	Invitrogen	18080051
Qubit dsDNA HS Assay Kit	ThermoFisher	Q32854
Deposited data		
Raw Caco-2 and LGG RNA sequences	NCBI's Sequence Read Archive (SRA)	PRJEB28403
RNA Sequencing R package/ analysis tool for generation of data/figures represented in this paper	This paper	https://git-r3lab.uni.lu/javier.ramirogarcia/nutrihumix.git
In silico scripts for generation of data/figures represented in this paper	This paper	https://github.com/ThieleLab/CodeBase/tree/master/Simulations_Greenhalgh_CellMetabolism_2019
In silico scripts for drug target identification represented in this paper	This paper	https://github.com/sysbiolux/NutriHuMiX
FASTCORMICS workflow	This paper	https://wwwen.uni.lu/research/fstc/life_sciences_research_unit/research_areas/systems_biology/software
Experimental models: Cell Lines		
Caco-2 cells	DSMZ	ACC169
Experimental models: Organism/Strains		
Lactobacillus rhamnosus GG (LGG)	ATCC	53103
Oligonucleotides		
Primers for RNaseq validation	This paper (Table S9)	N/A
Software and Algorithms		
MetaCore	Clarivate Analytics	Version 6.33 build 69110
In silico computing environment	MathWorks Inc.	MATLAB version 2016b
MATLAB toolbox for constraint-based modeling	COBRA Toolbox	https://github.com/opencobra/cobratoolbox
LGG ATCC 53013 reconstruction	AGORA	https://vmh.life 20.01.2017 Version 1.01.
COBRA Toolbox extensive for simulating interspecies interactions	Microbiome Modeling Toolbox	https://git.io/microbiomeModelingToolbox
In silico dietary regimens	Virtual Metabolic Human (VMH) Database	https://vmh.life
In silico dietary-specific regimens	This paper	https://github.com/ThieleLab/CodeBase/tree/master/Simulations_Greenhalgh_CellMetabolism_2019
sortmeRNA	Bonsai bioinformatics	Version 2.1
Subread (featureCounts)	Liao et al. 2014	Version −1.5.2 http://subread.sourceforge.net/
STAR	https://www.ncbi.nlm.nih.gov/pubmed/23104886	Version 2.5.2b https://github.com/alexdobin/STAR

(*Continued on next page*)

Continued

REAGENT or RESOURCE	SOURCE	IDENTIFIER
eggnog 4.5.	https://academic.oup.com/nar/article/44/D1/D286/2503059	http://eggnogdb.embl.de/#/app/home
Bowtie2	https://academic.oup.com/bioinformatics/advance-article/doi/10.1093/bioinformatics/bty648/5055585	Assembly ID: ASM2650v1 Version 2.3.0.
DESeq2 1.16.1	https://genomebiology.biomedcentral.com/articles/10.1186/s13059-014-0550-8	http://www.bioconductor.org/packages/release/bioc/html/DESeq2.html
Bcl2fastq	Illumina	Version 2.17.1.14
Drug target identification	https://www.drugbank.ca/	Version 5.0.10
GraphPad Prism 7	GraphPad	https://www.graphpad.com/scientific-software/prism
FlowJo software	BD Biosciences	Version 10
Metabolite Detector Software	https://omictools.com/metabolite-detector-tool	v3.020151231Ra
ELDA software	eld@	Version 4.12
Other		
Serum bottles (500 mL)	Glasgerätebau Ochs	Ref # 102091
Syringe	BD Biosciences	Ref #309110
Aluminum Crimp	Glasgerätebau Ochs	Ref 102050
Discofix 3 way stopcock (Serum bottle)	B.Braun	Ref 4095111
HuMiX gaskets	Auer precision	Design V3 Ref 21689-01 /-02/ −03
Human cell membrane (pore size: 50 nm)	Sigma-Aldrich (GE Healthcare)	Ref WHA111703
Bacterial cell membrane (pore size: 1 μm)	VWR (Whatman)	Ref 515-2084
Female Luer Lock to Barb Connector	Qosina	11733
Male Luer with Spin Lock to Barb	Quosina	11735
Polycarbonate lids (HuMiX)	University of Arizona	HuMiX 1.0.
Silicone tubing	VWR	Cat #228-0991
Marprene tubing (0,8 mm x 1,6 mm)	Watson-Marlow	Cat #14 #902.0008.J16
Manifold tubing	Watson-Marlow 984.0038.000	Cat # 14-284-151
Discofix 3-way stopcock	B.Braun	BRAU40951111
Needle (length: 25 mm; diameter: 0.60 mm)	VWR (color code: blue)	613-2017
Needle (length: 50 mm; diameter: 1.50 mm)	VWR (color code: red)	613-2031
Needle (length: 50 mm; diameter: 0.70 mm)	VWR (color code: black)	613-2020
Aeration cannula (length: 1,10; diameter: 30 mm)	VWR (B.Braun)	BRAU4190050
GC glass vials Magnetic caps	Chromatographie Zubehör Trott	40 11 00767 1011 23 716
Capillary column	Agilent J&W GC Column	DB-35MS
Anaerobic chamber	MBraun	Jacomex TepsLabo Edition 04/2008
Peristaltic pump	Watson-Marlow	Cat #205CA
Precellys® 24 homogenizer	Bertin instruments	PRECELLEYS 03119.200.RD000
Micro Pan Head Screw for thermoplastics	Newstar Fastenings	Length: 10 mm; Thread size: M2
FACSCanto II Flow cytometer	BD Biosciences	NA
CentriVap Concentrator 115V	Labconco	79773 Rev B, ECO 9574
Hungate tube and septum	VWR	Ref 78100-01
GC-MS System	Agilent Technologies	Agilent 7890A GC coupled to an Agilent 5975C MS
YSI Biochemistry Analyzer	YSI	2950D
Bioanalyzer	Agilent	2100

(*Continued on next page*)

Continued

REAGENT or RESOURCE	SOURCE	IDENTIFIER
Eppendorf ThermoMixer C	Eppendorff	Cat #5382000015
RNA-seq	Illumina	NextSeq500
LightCycler Instrument	Roche	480

CONTACT FOR REAGENT AND RESOURCE SHARING

Further information and requests for resources and reagents should be directed to and will be fulfilled by the Lead Contact, Paul Wilmes (paul.wilmes@uni.lu).

EXPERIMENTAL MODEL AND SUBJECT DETAILS

Human Cell Culture

The human epithelial CRC cell line Caco-2 (DSMZ: ACC169) were maintained in aerobic conditions at 37°C at 5% CO_2 in DMEM high glucose (Sigma-Aldrich) supplemented with 20% FBS (ThermoFisher).

Primary cell culture

Primary CRC tumor colon tissue was collected from an adenoma stage III CRC male patient by the Integrated Biobank of Luxembourg (IBBL, www.ibbl.lu) in accordance with institutional guidelines and has previously been described (Qureshi-Baig et al., 2016). All human samples used in the scope of this work were donated freely and written informed consent was obtained from the donor for the use of the sample for research. Ethical approval was obtained from the Comité National d'Ethique de Recherche, Luxembourg (Reference number 201009/09). Primary CRC cell T6 were maintained in aerobic conditions at 37°C in 5% CO_2 in DMEM-F12 (Westburg) supplemented with 10% FBS (ThermoFisher) and 1% Penicillin/Streptomycin (P/S; Lonza).

Bacterial cell culture

Lactobacillus rhamnosus GG (LGG) (ATCC: 53103) cultures were started from glycerol stocks kept at - 80°C and precultured overnight in Brain Heart Infusion Broth (BHIS; Sigma-Aldrich) supplemented with 1% hemin (Sigma-Aldrich) in hungate tubes (VWR) in an anaerobic chamber (MBraun) at 37°C, 5% CO_2 and < 0.1% O_2.

METHOD DETAILS

The HuMiX model

The assembly and setup steps of the HuMiX model have been described previously (Shah et al., 2016). In short, on day 1 after the HuMiX assembly, a 1 mL suspension of Caco-2 cells (6×10^5 cells/mL) in DMEM (Sigma-Aldrich) supplemented with 20% FBS (ThermoFisher) were injected into the epithelial chamber using a sterile disposable syringe (BD Biosciences) into the discofix 3-way stopcock (B.Braun) attached to a marprene tubing (Watson-Marlow) attached to the HuMiX inlet of the middle microchamber (Shah et al., 2016). After injection of Caco-2 cells on day 1, cells were allowed to attach to the collagen-coated (Invitrogen) microporous membrane (Sigma-Aldrich) at 37°C. 3 hours after the inoculation of cells, the peristaltic pump (Watson-Marlow) perfused DMEM medium at a flow rate of 25 $\mu L\ min^{-1}$ into the bacterial chamber and into the lower perfusion chamber. For 7 days, Caco-2 cells were continuously perfused with fresh DMEM medium from both apical (anaerobic medium) and basal side (aerobic medium), until a confluent Caco-2 monolayer was established (Shah et al., 2016). The anaerobic environment in HuMiX was maintained in the microbial microchamber at 0.1% by continuously bubbling the medium with dinitrogen gas. On day 7, after 24 hours preculture of LGG in BHIB (Sigma-Aldrich) in an anaerobic hungate tube (VWR), the bacterial cells were centrifuged at 5000 rpm for 7 minutes, and washed twice with PBS (Sigma-Aldrich). Then, 1 mL (OD ~1) of anaerobic bacterial suspension in DMEM (Sigma-Aldrich) supplemented with 20% FBS (ThermoFisher) was injected into the microbial microchamber onto the mucin-coated (Sigma-Aldrich) nanoporous membrane (VWR) as described above for human cells and the flow of the peristaltic pump continued to 25 $\mu L\ min^{-1}$, 30 minutes after bacterial inoculation (Shah et al., 2016). If the bacteria were provided with the simulated HF medium, the microbial microchamber in the HuMiX model was first primed for several hours with the HF medium, prior to the inoculation of bacteria. After a 24-hour co-culture of Caco-2 cells and LGG and the dietary regimen, the HuMiX experiment was terminated, the device was disassembled, and bacterial and human cells were collected from the microchambers (Shah et al., 2016). Two types of analyses were performed for each contingent whereby half of the biomass was used for biomolecular extraction, and a quarter was used for cell viability and count assessment performed by flow cytometry (BD Biosciences).

Biomacromolecular extraction

The biomolecular extraction for both Caco-2 and LGG cells have been described previously (Roume et al., 2013) (Shah et al., 2016). In short, Caco-2 cells were treated with a 1:1 methanol:water (v/v) solution (Merck), and polar and non-polar metabolite fractions were separated using chloroform (Merck). These fractions (containing intracellular metabolites) were snap-frozen and stored at - 80°C until use. The interphase containing DNA, RNA, and protein, were then processed using AllPrep DNA/RNA/Protein Kit (QIAGEN). The microbial cells were transferred to Precellys plastic vials containing 600 mg of 0.15-0.2 mm glass beads (Sigma-Aldrich), followed by lysis using Precelly's Homogenizer (Bertin Instruments). After cell lysis, polar and non-polar bacterial metabolite fractions were obtained by treatment with cold 1:3 methanol:water solution (v/v) (Merck). The bacterial interphase, including the glass beads (Sigma-Aldrich), were snap-frozen or processed directly using an All-in-One purification kit (Norgen). After extraction, biomolecules were stored at - 80°C until analysis.

Intracellular metabolite extraction

300 μL of the upper polar phase was transferred in technical duplicates into Gas chromatography mass spectrometry (GC/MS) glass vials (Chromatographie Zubehör Trott) and dried overnight at - 4°C in a CentriVap (Labconco). 150 μL of the lower non-polar phase was transferred in technical duplicates into GC/MS glass vials (Chromatographie Zubehör Trott) and dried overnight under a chemical hood. All GC/MS glass vials were capped and stored at −80°C until analyses. The remainder of the polar and non-polar phases was aliquoted in eppendorf tubes and stored at −80°C. 5-10 μL of the remainder of each sample was used for the quality control (QC) (pooling mixture) during GC/MS analysis.

Metabolite derivatization was performed using a multi-purpose sampler (GERSTEL). Dried polar sample extracts were dissolved in 20 μL pyridine, containing 20 mg/mL of methoxyamine hydrochloride (Sigma-Aldrich), and incubated under shaking for 120 min at 45°C. After adding 20 μL N-methyl-N-trimethylsilyl-trifluoroacetamide (MSTFA; Macherey-Nagel), samples were incubated for additional 30 min at 45°C under continuous shaking.

GC-MS analysis was performed by using an Agilent 7890B GC – 5977A MS instrument (Agilent Technologies). A sample volume of 1 μL was injected into a Split/Splitless inlet, operating in split mode (3:1) at 270°C. The gas chromatograph was equipped with a 5 m guard column + 30 m (I.D. 250 μm, film 0.25 μm) DB-35MS capillary column (Agilent J&W GC Column). Helium was used as carrier gas with a constant flow rate of 1.2 mL/min.

The GC oven temperature was held at 90°C for 1 min and increased to 270°C at 9°C/min. Then, the temperature was increased to 320°C at 25°C/min and held for 7 min. The total run time was 30 min. The transfer line temperature was set constantly to 280°C. The mass selective detector (MSD) was operating under electron ionization at 70 eV. The MS source was held at 230°C and the quadrupole at 150°C. Full scan mass spectra were acquired from *m/z* 70 to 700.

We applied an untargeted metabolic profiling approach in which the detected sample analytes were matched against an in-house library comprised of metabolites of the central carbon metabolism, as well as amino acid degradation/biosynthesis and or other related metabolites. Unidentified/undetected analytes are listed as "no match". All GC-MS chromatograms were processed using the MetaboliteDetector software, v3.020151231Ra (Hiller et al., 2009). The software package supports automatic deconvolution of all mass spectra, peak picking, integration, and retention index calibration. The following deconvolution settings were applied: Peak threshold: 5; Minimum peak height: 5; Bins per scan: 10; Deconvolution width: 5 scans; No baseline adjustment; Minimum 15 peaks per spectrum; No minimum required base peak intensity. Compounds were annotated by retention index and mass spectrum using the in-house mass spectral library.

Cell viability and counting

The mucin-coated bacterial membrane was first gently washed with PBS (Sigma-Aldrich) and resuspended in MACS buffer (PBS containing 1% BSA), then stained with the Live-dead Bac Light bacterial viability Kit (Life Technologies), followed by fixation with 3.7% Formaldehyde (Carl Roth). Quantification of bacterial cells was performed by flow cytometry (BD Biosciences) using approximately a 1:100 dilution of bacterial suspension and 10 μL of bacteria counting beads (ThermoFisher) as a standard for the volume of suspension. Caco-2 cells were stained with Live/Dead Fixable Near-IR Dead Cell Stain Kit (ThermoFisher) and fixed with 3.7% Formaldehyde (Carl Roth). The resulting data were analyzed using FlowJo software (BD Biosciences).

SCFAs extraction

The conditioned medium (cell-free supernatant containing soluble factors) was collected by centrifugation (4°C for 10 min at 12,000 *x* g) from 48-hour bacterial cultures in hungate tubes (VWR), aliquoted 5 × 750 μL into Eppendorf tubes, then snap-frozen and stored at −80°C until analysis. The extraction protocol of the SCFAs is based on an established protocol (Moreau et al., 2003). 20 μL of the internal standard (2-Ethylbutyric acid, c = 20 mmol/L, Sigma-Aldrich), were added to 180 μL of conditioned medium. After acidification with 10 μL of 37% hydrochloric acid (Sigma-Aldrich), 1 mL of diethyl ether (Sigma-Aldrich) was added and the samples were vortexed for 15 min at room temperature (Eppendorf Thermomixer). The upper organic phase was separated by centrifugation (5 min, 21,000 *x* g) and 900 μL were collected in a new reaction tube. A further 1 mL of diethyl ether (Sigma-Aldrich) was then added to the conditioned medium, and the tube was incubated and its contents separated by centrifugation. Then, 900 μL of the organic phase were combined with the first extract, and 250 μL of this combined mixture were transferred into a GC glass vial with micro insert (5-250 μL), in triplicate. For derivatization, 25 μL of N-tert-Butyldimethylsilyl-Nmethyltrifluoroacetamide (MTBSTFA)

with 1% tert-Butyldimethylchlorosilane (TBDMSCI, Restek) was added, and the samples were incubated for a minimum of 1 h at room temperature.

SCFAs measurement

GC-MS analysis was performed by using an Agilent 7890A GC – 5975C MS instrument (Agilent Technologies). A sample volume of 1 μL was injected into a Split/Splitless inlet, operating in split mode (20:1) at 270°C. The gas chromatograph was equipped with a 30 m (I.D. 250 μm, film 0.25 μm) DB-5MS capillary column (Agilent J&W GC Column). Helium was used as carrier gas with a constant flow rate of 1.4 mL/min.

The GC oven temperature was held at 80°C for 1 min and increased to 150°C at 10°C/min. Then, the temperature was increased to 280°C at 50°C/min (post run time: 3 min). The total run time was 15 min. The transfer line temperature was set to 280°C. The mass selective (MS) detector was operating under electron ionization at 70 eV. The MS source was held at 230°C and the quadrupole at 150°C. The detector was switched off during elution of MTBSTFA. For precise quantification, GC/MS measurements of the compounds of interest were performed in selected ion monitoring mode.

All GC-MS chromatograms were processed as described above.

Lactate measurement

Lactate from the LGG conditioned medium in either simulated HF or REF medium, as described above, were measured using a YSI Biochemistry Analyzer (YSI).

RNA library preparation for Caco-2 and LGG

Sequencing library preparation was performed using a NEBNext, Ultra Directional RNA Library Prep Kit (NewEngland Biolabs) using 500 ng of total RNA isolated from LGG or Caco-2 cells cocultured inside HuMiX under the described media conditions. Briefly, for bacterial RNA samples, ribosomal RNA depletion was carried out using a Ribo-Zero rRNA Removal Kit (bacteria) (Illumina) according to the manufacturer's protocol. Ribo-depleted RNA was purified using magnetic beads, resuspended into 5 μL of TE (Tris-EDTA) buffer and further processed for library preparation according to chapter 3 of the NEBNext, Ultra Directional RNA Library Prep Kit (NewEngland Biolabs) protocol booklet. The sequencing libraries for the Caco-2 RNA samples were prepared according to the protocol provided in chapter 2 of the NEBNext, Ultra Directional RNA Library Prep Kit (NewEngland Biolabs). The libraries were quantified using a Qubit dsDNA HS Assay Kit (ThermoFisher), and quality was determined using the bioanalyzer (Agilent). Pooled libraries were sequenced on a NextSeq500 sequencer using 2 × 75 cycle reaction chemistry. FASTQ file generation and demultiplexing were performed using bcl2fastq (Illumina).

Simulated media preparation

Two types of simulated dietary regimens were used in our study. The high-fiber (HF) medium is a modification from the simulated ileal environment medium (SIEM) (Gibson et al., 1988). SIEM medium contained 47 g/L bactopeptone (BD Biosciences), 78.4 g/L potato starch (Sigma-Aldrich), 9.4 g/L xylan (Sigma-Aldrich), 9.4 g/L arabinogalactan (Sigma-Aldrich), 9.4 g/L amylopectin (Sigma-Aldrich), 9.4 g/L pectin (Sigma-Aldrich), 3 g/L casein hydrosylate (Sigma-Aldrich), 0.8 g/L dehydrated bile (Sigma-Aldrich), and 4 g/L soy (Frutarom). All components were dissolved in distilled water with the help of a magnetic stirrer and heat (120°C). The medium was autoclaved at 121°C, and 10 mL/L trace minerals (ATCC), 10 mL/L Vitamin mix (ATCC), menadione (Sigma-Aldrich) and 100 mM cysteine HCl (Sigma-Aldrich) were filter-sterilized and added to the autoclaved medium. Menadione was dissolved (1 mg/mL) in DMSO (Sigma-Aldrich) prior to being added to the medium. After achieving complete homogeneity, the pH was adjusted to 7.0 using HCl and NaOH (Sigma-Aldrich). The medium was conserved in 50 mL aliquots at - 20°C until use. Before use, the medium was thawed at 37°C, transferred to a serum bottle with a rubber stopper (VWR), and made anoxic by 48 hour incubation in an anaerobic chamber (M.Braun). The no-dietary-fiber medium, termed the reference (REF) medium, was Dulbecco's Modified Eagle's medium (DMEM) (Sigma-Aldrich) supplemented with 20% FBS (ThermoFisher), as it provides the basic requirements for culture of both Caco-2 cells and LGG (Shah et al., 2016).

Sphere and 3D colony formation assays

Self-renewal capacity was assessed with sphere formation assays, as previously described (Qureshi-Baig et al., 2016). Briefly, primary CRC cells T6 (IBBL) and Caco-2 cells were seeded at different densities (e.g., 1, 2, or 3 cells per well), and after 10 days of culture, the resulting spheroids were counted and measured under a microscope. Extreme limiting dilution analysis (ELDA) software (Hu and Smyth, 2009) was used to determine the self-renewal capacity after a given treatment. 3D colony formation was assessed by resuspending the cells in a serum-free a mix of 60% Sphere Culture Medium (SCM) (Qureshi-Baig et al., 2016) and 40% methylcellulose medium, i.e., MethoCult ® H4100 (STEMCELL Technologies) medium, supplemented with 20 ng/mL Epidermal Growth Factor (EGF; Biomol) and 20 ng/mL basic fibroblast growth factor (bFGF; Miltenyi Biotec). The SCM medium was composed of DMEM-F12 (Westburg), 20 μL/mL of B27 (ThermoFisher), 2 μL/mL of insulin (Sigma-Aldrich), 3.4 μL/mL of glucose (Sigma-Aldrich), 4 μg/mL of heparin (Sigma-Aldrich), and 10 μL/mL of 1% P/S (Lonza). 250 cells per well (per 35 mm dish) were seeded. The resulting colonies were counted after 14 days, using an inverted microscope.

qRT-PCR validation

cDNA synthesis was performed on Caco-2 RNA samples from HuMiX using the Superscript Synthesis kit (Invitrogen). qRT-PCR was performed on *abcc3, abca5, abcc2, cox-2*, *traf6*, and *c-Jun* using SYBR Green Supermix (Bio-Rad) and processed according to the protocol booklet using HPRT1 and GAPDH as housekeeping genes. The primer sequences can be found in Table S9. Thermocycling parameters were 95°C (5 min; denaturing step), followed by amplification 95°C (15 s), 60°C (40 s), and 72°C (30 s). A total of 50 cycles were performed. Reactions were performed on LightCycler Instrument (Roche).

In silico model predictions

Simulations were performed in MATLAB version 2016b (MathWorks, Inc.) using the COBRA Toolbox 3.0, version 31.05.2018 (Heirendt et al., 2019) (https://opencobra.github.io/). Computationally efficient flux variability analysis (Gudmundsson and Thiele, 2010) was performed with the IBM CPLEX (IBM, Inc.) solver. A context-specific COAD model was reconstructed using the human genome-scale metabolic reconstruction Recon2 (Thiele et al., 2013) and data from the TCGA dataset, an adaptation of the FASTCORMICS workflow for RNA-seq data (Vlassis et al., 2014). The uptake reactions of Recon2 were first constrained in relation of the media composition. Then, FASTCC (Vlassis et al., 2014) was run to remove any inconsistent reactions. The medium-constrained Recon 2 model and the expression data from COAD patients from the TCGA dataset were used as input for a modified version of FASTCORMICS workflow (Pacheco et al., 2015) that allows processing of RNA-Seq datasets.

In silico diet-host-bacteria reconstruction

The COAD and LGG model were constructed using the createMultiSpeciesModel function in the Microbiome Modeling Toolbox (Baldini et al., 2018) which was implemented in the COBRA Toolbox (Heirendt et al., 2019). Briefly, the two models were joined through a shared compartment representing the intestinal lumen, which enabled cross-feeding and served as an inlet for the simulated medium and an outlet for the secretion of metabolic end products. The fluxes through all metabolic and transport reactions in each joined model were coupled to the flux through its biomass objective function (Heinken et al., 2013). The models were contextualized as follows: (i) Growth rates calculated from cell counts measured *in vitro* were used as lower and upper bounds on the respective species' biomass objective functions in the conditions with experimental data available. If cell count measurements for Caco-2 were not available, a growth rate of 0.01 h^{-1} was assumed. (ii) Semiquantitative measurements for acid production by LGG in a single culture were integrated by enforcing the ratio between acetate and formate production to the measured ratios (iii). The respective medium (HF or REF) was implemented as constraints on the exchange reactions to the lumen compartment, which represents the apical side of HuMiX. In each simulation including the human cell, the DMEM medium was additionally implemented as constraints on the body fluid exchange reactions, which represent the basal side of HuMiX. Uptake of O_2 by COAD cells was allowed by setting the lower bounds on the body fluid O_2 exchange reaction to −100. To ensure anoxic conditions on the luminal side, O_2 uptake via the lumen compartment was prevented by setting the lower bound on the lumen O_2 exchange reaction to zero. The reference and simulated HF media were adapted as *in silico* constraints by translating the dietary components into the corresponding Virtual Metabolic Human (https://vmh.life) metabolite identifiers and estimating the uptake rates based on the *in vitro* composition (Noronha et al., 2019). Scripts used to perform simulations are provided in https://github.com/ThieleLab/CodeBase/tree/master/Simulations_Greenhalgh_CellMetabolism_2019.

Drug target identification

For the drug target identification, a pipeline was established that automatically retrieved gene and drug interactions as well as their relation to cancer (Adapted from (Pacheco et al., 2015)). The pipeline retrieves data from selected databases and was implemented in MATLAB 2017b. As input, a list of Ensembl identifiers (or other) is sufficient. The pipeline converted the Ensembl identifiers into the official gene symbol as well as UniProt identifier. A list of corresponding IDs can be retrieved from the HUGO Gene Nomenclature Committee website (available at https://www.genenames.org/cgi-bin/download) and Biomart (provided by Ensembl, available at http://www.ensembl.org/biomart/martview/). The UniProt identifiers were then used to retrieve drug target information from the DrugBank (Release Version 5.0.10 available at https://www.drugbank.ca/), a freely accessible database that contains information on more than 10,510 drugs as well as their targets. The *urlread* command from MATLAB 2017b allowed to search for each UniProt identifier (by combining the website URL with the UniProt identifier) in the DrugBank in order to read the source code and to extract the names and BE identifiers using regular expression (*regexpi* command). The process was repeated using the BE identifiers to retrieve protein-drug associations along with the drug name, the drug group (e.g., approved, experimental, nutraceutical, illicit, withdrawn, and investigational), actions (e.g., inhibitor, substrate, activator, and inducer) and, most importantly, the drug identifiers. The pipeline then retrieved, for each drug identifier (using the same approach), information on the drugs, such as drug categories and KEGG drug identifiers for pathway extraction using regular expression on the source code. The KEGG identifiers (http://www.genome.jp/dbget-bin/www_bget?drug:D02368) were used to retrieve human-related pathways. In the last step, cancer drug databases and other online resources were downloaded from different sources including cancer.gov (maintained by the National Cancer Institute, available at https://www.cancer.gov/about-cancer/treatment/drugs), Chemocare (reviewed by the Cleveland Clinic and community resources, available at http://chemocare.com/chemotherapy/drug-info/default.aspx), CenterWatch (information about clinical trials and FDA approved drugs, available at https://www.centerwatch.com/drug-information/fda-approved-drugs/therapeutic-area/12/oncology), NavigatingCare (mostly patient based, available at https://www.navigatingcare.com/library/all/chemotherapy_drugs),

SEER*Rx (antineoplastic drug database maintained by the National Cancer Institute, available at https://seer.cancer.gov/tools/seerrx/) and Cancer Research UK (a cancer research and awareness charity, available at http://www.cancerresearchuk.org/about-cancer/cancer-in-general/treatment/cancer-drugs/drugs). Then, regular expression was used to compare the drug names generated by the pipeline and the downloaded resource.

QUANTIFICATION AND STATISTICAL ANALYSIS

All statistical details of the *in vitro* experiments are described in the figure legends. Additional descriptions of software, packages and algorithms employed for the analysis of RNA sequencing data and *in silico* simulations are described below:

Intracellular metabolomics analysis

Because we could not assume equal variances for both conditions (simulated HF regimen versus REF medium, +/− LGG) and to increase the statistical power by taking into consideration Type 1 as well as Type 2 error rates, we applied the Welch's t test for metabolomics data analysis (Ruxton, 2006). The Welch t test provides more robustness to an analysis than the regular Student t test, and thus, the Welch t test is commonly applied in metabolomics datasets (Kogel et al., 2010; Theriot et al., 2014). Statistical analyses were performed separately by comparing dietary regimen (HF versus REF) and dietary regimen + LGG (HF + LGG versus REF + LGG). Bacterial intracellular metabolites were analyzed by comparing HF + LGG versus REF + LGG. A P value of less than 0.05 was considered significant for all analyses. Metabolite replicates with one 'no match' hit technical replicate were removed from the dataset. A total of 155 metabolites were detected in Caco-2 cells in each condition. 50 statistically significant metabolites were identified in HF-exposed versus REF-exposed Caco-2 cells (See also Table S1); 44 statistically significant metabolites were identified when Caco-2 cells were exposed to HF + LGG versus REF + LGG (See also Table S5); 33 statistically significant metabolites were identified in LGG when exposed to HF versus REF medium (See also Table S4).

SCFA quantification

For SCFAs absolute quantification, an external calibration curve (10, 25, 50,100, 250, 500, 1000, 2000, 4000 μmol/L) using a volatile free acid mix (Sigma-Aldrich) including all compounds of interest was prepared, extracted, and derivatized as described above. A total of four volatile acids were measured in the LGG spent medium: Acetic acid, butyric acid, formic acid, and propionic acid. The absolute quantification of each metabolite produced by LGG was performed in the medium with background subtraction from fresh medium and normalized to cell count.

In silico analysis

Simulations were performed on the two dietary regimens for (i) the COAD model, (ii) the LGG model, and (iii) the joint COAD/LGG model. In each of these six conditions, the minimal and maximal fluxes through each reaction were computed using a computationally efficient flux variability analysis (Gudmundsson and Thiele, 2010). For each reaction, the flux span was calculated, which is the absolute distance between the computed minimal and maximal flux values. The minimal and maximal fluxes for each reaction were plotted in MATLAB. The predicted secretion into the body fluids and lumen were visualized using the *pheatmap* and *RColorBrewer* functions in R version 3.3.2 (R Core Team, 2016). Heatmaps were generated with the Euclidian distance measure for clustering rows and columns, and complete linkage as the hierarchical clustering method. Reactions with at least a 20% difference in flux span between conditions were plotted. The thicknesses of the lines per reaction were scaled to fold changes in the flux spans between conditions.

RNA-sequencing analysis

To ensure complete removal of all rRNA in the bacterial samples, we performed *in silico* rRNA depletion using sortmeRNA (Bonsai Bioinformatics) (Kopylova et al., 2012). For the human samples, rRNA depletion was not performed as only mRNAs were sequenced. The rRNA depletion was required only for the bacterial samples, as rRNA made up 85% of the total RNA, to avoid that all other RNA classes are masked (Rosenow et al., 2001; Scott et al., 2010). The remaining reads were mapped to the LGG reference genome using bowtie2 (BOWTIE) (Langmead and Salzberg, 2012) with a default setting at the very-sensitive-local mode. The reference genome was reannotated using eggnog-mapper based on eggNOG 4.5 orthology data (Huerta-Cepas et al., 2017), and gene counts were strand based, applying an in-house script.

Differential expression analysis

The DESeq2 (1.16.1) (Anders and Huber, 2010) package from R (3.4.1) (R Core Team, 2016) was used to identify genes that were differentially expressed (DE) due to dietary regimen. In a similar approach, Caco-2 transcriptomic datasets were aligned against the Ensembl human genome reference (release-87) using the STAR (2.5.2b) aligner (Dobin et al., 2013) with default parameters, except for chimSegmentMin, which was set to 20 to switch on the detection of chimeric alignments. A GTF file (release-87) with the annotated transcripts was also provided to increase the accuracy of the alignments. Gene counts were calculated using featureCounts (v1.5.2) (Liao et al., 2014), requiring both ends to be mapped as well as strand specificity. To filter out genes that could be derived from spurious mapping, only genes that collected at least 0.0001% of the reads for a minimum of two samples

from the same condition were retained. Generalized linear models were applied to calculate the differential gene expression and statistical significance per dietary regimen, type of culture (monoculture or coculture) and their interaction using DESeq2 (Anders and Huber, 2010). Figures for LGG and Caco-2 transcriptomic analysis were generated using the R packages gplots, superheat, ggplot2 and tidyverse.

Pathway enrichment analysis

Pathway enrichment analysis on the Caco-2 differentially expressed gene list (simulated HF regimen versus REF medium, and HF + LGG versus REF + LGG) was performed using MetaCore (Clarivate Analytics), using only the statistically significant genes as a sorting method. DE genes with an absolute $\log_2$-fold change value higher than 1 and an adjusted P value lower than 0.05 were used as a sorting method for Caco-2 cells. LGG pathway and module enrichment was performed using the R packages KEGGREST (Tenenbaum, 2017) and stats (R Core Team, 2017) (hypergeometric distribution function). Figures for LGG and Caco-2 transcriptomic analysis were generated with the R packages gplots, superheat, ggplot2 and tidyverse.

DATA AND SOFTWARE AVAILABILITY

All metabolomic data as well as the output files from the pathway analysis are freely available in Supplemental Files. Transcriptomic raw sequences are available at NCBI's Sequence Read Archive (SRA) under Project PRJEB28403. The transcriptomic analyses codes are available on github (https://git-r3lab.uni.lu/javier.ramirogarcia/nutrihumix.git). All *in silico* scripts are publicly available and can be found in the repository under https://github.com/ThieleLab/CodeBase/tree/master/Simulations_Greenhalgh_CellMetabolism_2019. The AGORA (Magnúsdóttir et al., 2017) reconstruction of LGG ATCC 53103 (version 1.01) is available on https://vmh.life 20.01.2017. The drug prediction codes are publicly available and can be found in the repository under https://github.com/sysbiolux/NutriHuMiX. The FASTCORMICS workflow is available under https://wwwen.uni.lu/research/fstc/life_sciences_research_unit/research_areas/systems_biology/software.